A comprehensive model for the supported vanadium oxide catalyst: *The umbrella model*

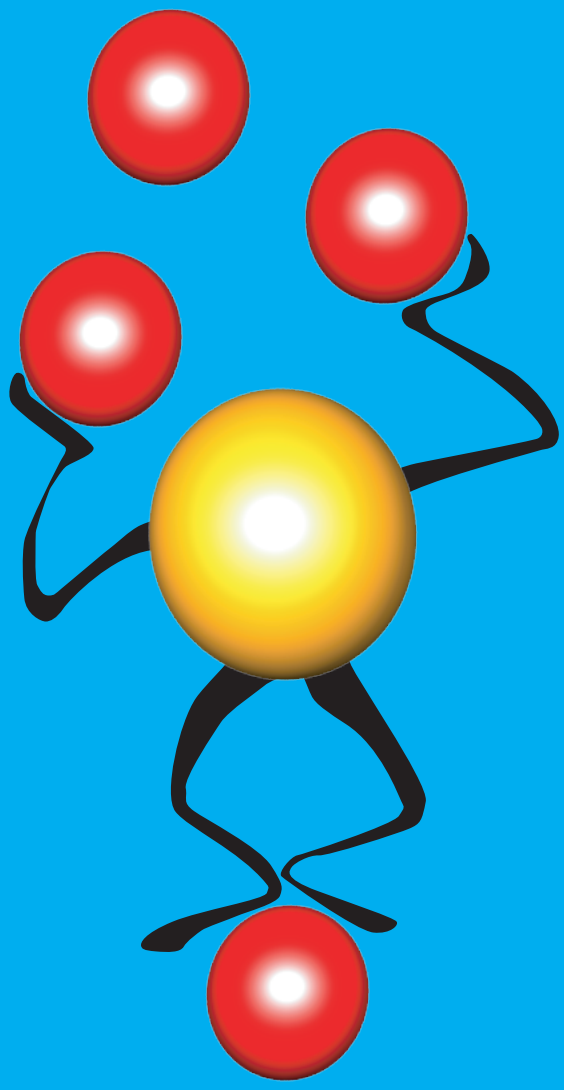

Joost van Lingen

A comprehensive model for the supported vanadium oxide catalyst: The umbrella structure

J.N.J. van Lingen

Colofon

ISBN-10	90-393-4371-3
ISBN-13	978-90-393-4371-5
Printer	Ponsen en Looijen B.V. Wageningen

Cover	J.N.J. van Lingen

A comprehensive model for the supported vanadium oxide catalyst: The umbrella model

Een veelomvattend model voor
de gedragen vanadium oxide katalysator:
Het paraplu model

(met samenvatting in het Nederlands)

Proefschrift

ter verkrijging van de graad van doctor aan de Universiteit Utrecht op gezag van de rector magnificus, prof. dr. W.H. Gispen, ingevolge het besluit van het college voor promoties in het openbaar te verdedigen op maandag 27 november 2006 des middags te 2.30 uur

door

Joost Nelis Johannes van Lingen

geboren op 29 oktober 1977 te Zeist

Promotor: Prof. Dr. Ir. B.M. Weckhuysen

Co-promotoren: Dr. J.H. van Lenthe
Dr O.L.J. Gijzeman

Contents

Chapter 1

General introduction

1.1 Catalysis

The word catalysis is used to describe a process in which the rate of formation of a chemical product in a reaction is increased or decreased by adding a substance, the catalyst. In principle, this substance is not altered or consumed by the reaction[1]. Figure 1.1 illustrates this concept for the reaction AB + C → A + BC. The reaction without catalyst has to go over a high energy barrier to form the product. First the bond between AB has to be broken or at least weakened before the bond between reactants B and C can be formed. In a simplified view the energy difference between the starting level of the reaction and the maximum in the curve is the activation energy (ΔE_{act}). The higher this energy the more limited the reaction rate will be or the reaction may not occur at all to a measurable degree. When the catalyst is added the energy barrier is lowered; in other words, the process needs less activation energy and this increases the chance of the reaction to happen. This is called the *activity* of the catalyst.

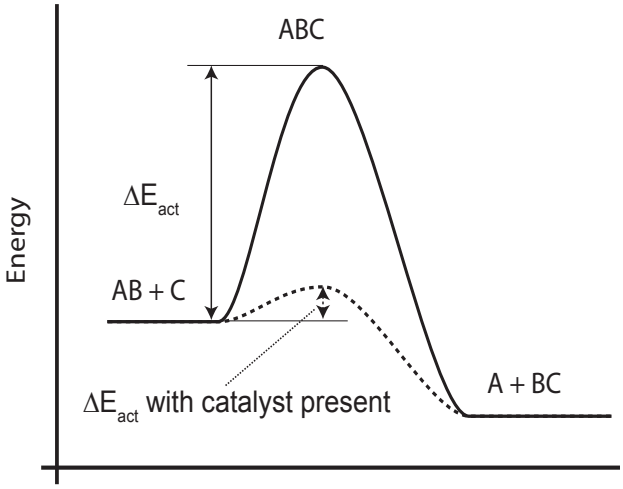

Figure 1.1 Energy diagram for the reaction AB + C → A + BC.

Originally the word catalysis is derived from the Greek noun κατάλυσις, related to the verb καταλύειν, meaning *to annul* or *to untie* or *to pick up*. In 1836 the word catalysis was used for the first time in relation with chemical reactions by Berzelius, who coined it to describe what he thought to be a new force acting during a chemical reaction[1,2]. However, catalytic processes have been around for ages. For example, the production of beer has been dated back to 7000 B.C. and beer is produced via a fermentation process, which is catalyzed by an enzyme, the catalyst of nature[3]. That these processes were used did not mean that they were really understood. In the end of the 18th century and the beginning of the 19th century scientists started to study the influence of metals and oxides on several decomposition processes[2]. It was found that for different metals different products were produced. For example, ethanol is decomposed into carbon and an, at that time unknown, uninflammable gas in the presence of copper and iron. In contrast, when pumice stone is present ethanol decomposes into ethene and water[2]. This brings forward the second characteristic of a catalyst: *selectivity*. It increases the change of producing one kind of compound.

A catalyst can be any kind of material that influences a reaction in a positive way, meaning that it increases the reaction rate or the selectivity for one of the possible products and eliminating the side products. The catalyst can do its work in a homogeneous or in a heterogeneous surrounding. In the former case the catalyst and the reactants are in the same phase for example all liquids or gasses. This means most of the time that, although the catalyst is not consumed by the actual reaction, it cannot be reused since it is included in the product phase. In the case of a heterogeneous catalyst, the reactants in the gas or liquid phase are passed over a solid catalyst[4]. In theory this can go on indefinitely. However, catalysts sometimes, if not always, get deactivated. They need then to be reactivated[1]. This gives the third characteristics of a good catalyst, *stability.* A catalyst should have a long lifecycle. So a catalyst makes one of the possible reactions more favorable (*selectivity*), works a long time (*stability*) and increases the reaction rate (*activity*) in that order of importance[1].

Suitable catalysts for reactions involving O_2 are composed of transition metals. In such reactions O_2 has to go from its ground state, which is a triplet (two unpaired electrons), to a singlet state. This transition is forbidden by spin selection rules. The transition metals have, however, large spin orbit couplings. This coupling makes the selection rules to soften so that the O_2 molecule can cross over to the singlet state and take part in the reaction. An example of such transition metal-based catalysts is vanadium oxide, which represents the topic of this PhD thesis.

1.2 Vanadium oxide-based catalysts

The element vanadium was discovered in 1801 by a Spanish mineralogist A.M. del Rio. He called it Erythronium. Thirty years later the element was rediscovered by a Swedish chemist named N.G. Sefström who named it after the goddess Freya for whom Vanadis is an old Norse name. This is the name it still has today[5].

Vanadium is one of the most abundant metals on earth and is found in lots of minerals, certain ores and also in organic complexes like crude oil. The element is mostly used as an additive in steel and alloys to improve the quality of the produced material. Next to this metallurgical application vanadium oxides are heavily used in catalysis industry. Vanadium oxide-based catalysts are used to produce several important chemicals and in the reduction of environmental pollution[5]. Table 1.1 gives an overview of the usage of vanadium oxides as presented in the catalysis literature.

Most of the vanadium oxide-based catalysts consist of a VO_x phase deposited on a oxidic support, like SiO_2, Al_2O_3, TiO_2 and ZrO_2. They are named supported vanadium oxide catalysts. Initially this support was added to increase the surface area of the vanadium oxide phase and so the activity of the catalyst, with the support having seemingly no influence on the catalytic action. However, in the last decades it has been found that the support has

Table 1.1 An overview of chemical processes involving vanadium oxide-based catalysts based on a review paper of Weckhuysen and Keller[5].

Selective oxidation of alkanes and alkenes
Selective catalytic reduction of NO_x with NH_3
Oxidation of o-xylene to phthalic anhydride
Ammoxidation of aromatics and methylaromatics
Selective oxidation of methanol to formaldehyde
Oxidation of SO_2
Decomposition of isopropylalcohol
Oxidation of aliphatic and aromatic hydrocarbons
Photo-oxidation of CO
Photo-isomerization of butane
Partial oxidation of methane to formaldehyde
Oxidation of H_2S
Synthesis of isobutyraldehyde from methanol and ethanol
Selective oxidation of 4-methylanisole
Selective oxidation of p-methoxytoluene
Alkylation of aldehydes with methanol
Oxidative coupling of methane
Synthesis of 2,6-dimethylphenol from methanol and cyclohexanone
Synthesis of isobutyraldehyde from methanol and *n*-propylalcohol
Total oxidation of benzene
Dehydrocyclodimerization of isobutene to xylene
Polymerization of olefins
Selective oxidation of alkanes with peroxides
Oxidative dehydrogenation of alkanes
Isomerization of *m*-xylene
Epoxidation of alkenes with peroxides
Hydroxylation of phenol
Direct conversion of methane to aromatics

a significant influence on the active catalyst species on top of that support. Differences in activity and selectivity were recorded when the same synthesis route was used to deposit the active phase of V_xO_y on top of another support. For example, the activity for an oxidation reaction like methanol to formaldehyde, which will be discussed in Chapter 5, the turn over frequency (TOF) for the supports ZrO_2 and TiO_2 is three orders of magnitude higher than for SiO_2[6]. The exact mechanisms for these metal oxide-support interactions are still unknown. Catalysis over vanadium oxide-based catalyst or catalysis in general is a very complex process. Small changes in geometrical structure and related to that electronic structure will change the performance of the catalyst material.

This sensitivity shows that it is possible to finetune an existing catalyst in activity, selectivity and stability, which is one of the main goals of the research in the field of catalysis, next to the development of new catalysts that can be used for the production of new bulk and fine chemicals, in environmental issues like the reduction of NO_x[5,7]. Before it is possible to do this fine tuning a good fundamental understanding of the molecular structure and working of the catalyst has to be developed. In the last decades researchers have tried to elucidate the molecular structure of vanadium oxide catalysts by various spectroscopic techniques, including IR, Raman, UV-VIS, EXAFS and NMR. An example of a review of these results has been published by Wachs and Weckhuysen[8]. On the basis of these experimental data and those of reference compounds, from which the molecular structure was known, model structures where developed that should be capable of reproducing the experimental data. In what follows, we will discuss the different models presented in the literature for supported vanadium oxide catalysts.

1.3 Molecular models for supported vanadium oxide catalysts

The experimental search for the molecular structure of vanadium oxide-based catalysts started with studies of bulk V_2O_5 and its catalytic properties in the beginning of the 1940's. Supported vanadium oxide catalysts consist of an active vanadium oxide phase on top of a support. Depending on the loading crystalline V_2O_5 is formed on the support, easily recognizable by a sharp peak[9,10] in the Raman spectra at 994 cm^{-1}, or dispersed monomeric or polymeric V_xO_y species[8]. This thesis focuses on isolated monomeric VO_4 species. So only low-loaded supported vanadium oxide catalysts will be considered in the further discussion. Around 1980 the first reports[11-16] appeared in literature about a V=O species which is characterized by a peak in IR and Raman spectra around 1030 cm^{-1}, assigned to the V=O stretch vibration. Other reports in that same time period showed that the monomeric structure is a distorted tetrahedron[16-20]. Next to these general features more specific structural models for the monomeric VO_4 species can be found in the literature. The main difference between these models is the way the tetrahedral VO_4 species is attached to the surface of the support.

The distorted tetrahedron has four O-atoms surrounding the central V-atom. One of these O-atoms has to be doubly bound, so that three O-atoms can possibly be a part of a V-O-M (M stands for the cation in the oxidic support) bond. These V-O-M bonds are formed by reaction of the VO_x species with the hydroxyl groups on the surface of the support when the species is deposited[5]. This gives automatically the following models:

A) The pyramid model, introduced in the 1980's, (Figure 1.2A), with three Si-O_s-V bonds connecting it to the surface of the support and a single V=O bond on top is the most popular one[10,11,19,21-24]. It is not that surprising that this model was proposed. It is probably the first thing that comes to mind when placing a tetrahedron of VO_4 on an oxidic surface.

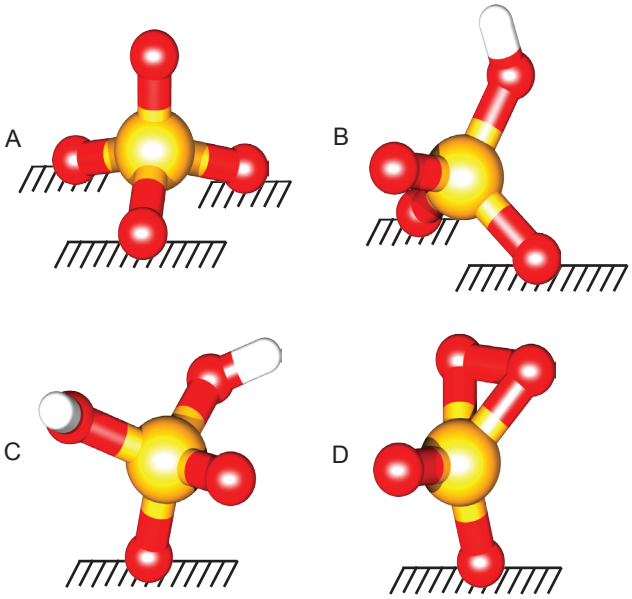

Figure 1.2 Models for the supported vanadium oxide species. In yellow the V-atoms, red the O-atoms and white the H-atoms.

B) A two legged structure. In the literature two models with two bonds to the support can be found. Kozlowski et al.[18] proposed a molecular structure, which has two Si-O_s-V bonds and two V=O bonds. This structure has been discarded as a candidate structure by Bond et al.[25] and later on by EXAFS experiments[26,27], which showed that there is one O-atom at 1.58 Å and 3 O-atoms at a distance of 1.78 Å from the central V-atom. The O-atom at the shorter distance being the doubly bound O. When the model, with two V=O bonds, was rejected by Bond et al. they presented a hydrogenated variant of this structure (Figure 1.2B) where one of the V=O bonds is replaced by a V-OH as a possible structure[25,28-31].

C) A singly bound model has been presented by Van der Voort et al.[32] This molecular structure (Figure 1.2C) has a V=O group, two OH groups and a single bond to the support.

All of these models fulfill the necessary requirements mentioned above of being a distorted tetrahedron and having a V=O group to explain the presence of the peak at 1030

cm^{-1} in the Raman spectra. They will, however, have there own spectroscopic characteristics which should make it possible to distinguish between them. We will discuss this further in Chapters 3 and 4.

1.4 Scope of the thesis

From the fact that these molecular structures mentioned above for monomeric VO_4 are still proposed in the literature up to now, it can be concluded that there is yet no definite model for supported vanadium oxide catalysts and that perhaps there are not one, but two or three species that can be present at a surface. That after 20 years of spectroscopic research this discussion is still open, shows that the elucidation of the molecular structure of supported vanadium oxide-based catalysts based on spectroscopic techniques alone has reached its limits. The goal of this thesis will be to study the molecular structure of supported vanadium oxide catalysts in a different way by combining the experimental data from literature with the predicting power of quantum chemistry. This scientific tool has been around since the 1920's and has the capability to compute molecular properties for model structures. However, until the 1990's it lacked the computing power to do this with a reasonable precision on large enough cluster models that, in our opinion, are needed to mimic the molecular structure of a heterogeneous catalyst. With the introduction of density functional theory (DFT)[33] in combination with the increasing availability of computational power and the release of parallelized computational programs like GAMESS-UK[34] it is now possible to do reliable calculations on possible structures of catalyst materials and their reaction mechanisms. Still, when work started on this thesis in the beginning of 2002, there were very few theoretical studies[29,35] on the molecular structure of monomeric VO_4 species.

As said above model structures are needed to compute molecular properties. In our opinion the set of potential models for the supported vanadium oxide catalysts in the literature is not complete. The possibility that there is only one bond to the support is for example almost completely ignored. Only Van der Voort et al.[32] proposed such a structure (Fig 1.1C), based on IR spectroscopy. We will introduce in Chapter 2 another model with one bond to the alumina support, shown in Figure 1.2D, where the vanadium atom is linked to the surface *via* only one Al-O_s-V bond and further consists of a V=O and a perturbed O_2 molecule linked to the central vanadium atom. We named this model the umbrella model[27,36,37]. Chapter 3 contains a more detailed study into the umbrella model using silica as a support.

After the introduction of the umbrella model in Chapters 2 and 3 a comparison between the models already in the literature and the umbrella shown in Figure 1.1 will be made in Chapter 4. The calculated IR and Raman spectra of the models will be discussed and compared with experimental IR and Raman data.

In Chapter 5 we will discuss possible reaction mechanisms for selective oxidation reac-

tions based on this umbrella model. As an example the formation of formaldehyde from methanol over supported vanadium oxide catalysts will be used. In this reaction mechanism the initial state is a triplet since an oxygen molecule is one of the reactants. The final state is a singlet. This means that the oxygen molecule has gone from a triplet to a singlet state. This transition is forbidden by the selection rules. However vanadium has a large spin orbit coupling, which makes the selection rules less absolute. Spin orbit coupling is a relativistic effect. In Chapter 6 we have a first study into the need to incorporate relativistic effects by applying the ZORA (Zeroth Order Regular Approximation) module in GAMESS-UK[34] on several known relativistic compounds as well as the umbrella model.

1.5 A uncommon tool in catalysis: quantum chemical calculations

Quantum chemical calculations are a large part of this thesis. Some basic knowledge of these methods is therefore required to fully understand the following Chapters. In the following a short introduction is given.

Formally to calculate the molecular properties of the models presented in Figure 1.2, like IR and Raman spectra, first the wave function of the system, ψ, has to be obtained by solving the Schrödinger equation (Eq 1.1) for these models:

$$H\psi = E\psi \tag{1.1}$$

Here is H the Hamilton operator and E the energy of the system. However, it is only possible to solve the Schrödinger equation for one electron systems like; H, H_2^+ and He^+. So we have to rely on approximate methods. In this thesis we use mainly the HF (Hartree Fock)[38-40] and DFT (density functional theory)[33] methods as included in GAMESS-UK[34], which are single determinant methods. HF uses instead of the Hamilton operator the Fock operator, which is a one electron operator and includes the average repulsion with the remaining electrons in the system. By definition it has no correlation energy. DFT uses the Kohn-Sham operator, similar to the Fock operator except that the exchange operator is replaced by a functional. The B3LYP[41,42] functional was used in this thesis.

When the wave function is known molecular properties can be calculated by letting the operator for this molecular property act on the wave function. This can be written as:

$$\langle \psi | p | \psi \rangle \tag{1.2}$$

with p being the operator for a specific molecular property.

As an example we take the umbrella model (Figure 1.2C). The cluster model first has to be optimized, which means that the internal distances are varied to minimize the total energy of the system. The program walks over the potential surface in all directions to find a minimum, using the gradient of the energy as guidance. The change in energy is described

by the following formula[43], which is a Taylor expansion in the displacement of the nuclear coordinates R_i from their equilibrium position $R_{i,0}$.

$$E(R) = E(R_0) + \sum_i \left(\frac{\partial E}{\partial R_i}\right)(R_i - R_0) + \sum \left(\frac{\partial^2 E}{\partial R_i \partial R_j}\right)(R_i - R_0)(R_j - R_0) + ... \quad (1.3)$$

It is convenient to change from the coordinates R_i to normal coordinates Q_i. These involve the masses of the nuclei as well. This makes the energy a quadratic function to second order in the nuclear displacement[44]:

$$E(Q) = E(Q_0) + \sum_i \left(\frac{\partial E}{\partial Q_i}\right)(Q_i - Q_0) + \sum_i \left(\frac{\partial^2 E}{\partial Q_i^2}\right)(Q_i - Q_0)^2 + ... \quad (1.4)$$

A minimum has been found if the first derivative, the gradient, is zero and all the second derivatives, the Hessian, are positive. The internal distances found, can then be compared with results from e.g. EXAFS experiments, which gives the distances from the central V-atom to surrounding atoms and the type of surrounding atom. For the umbrella model an example of this comparison is given in Table 1.2.

Table 1.2 Computed internal distances for the optimised umbrella model, Figure 1.2D, compared with EXAFS results. In brackets the coordination number for the atoms at this distance resulting from the EXAFS experiments or the DFT calculations is given.

Bond	**Umbrella Model** (Å)	**EXAFS** (Å)
V=O	1.580 (1)	1.59 (1)
V-O	1.799 (2)	1.77 (3)
V-O_s	1.778 (1)	

After the optimization the vibrational modes of the model can be calculated from the Hessian:

$$\frac{\partial^2 E}{\partial Q_i^2} \quad (1.5)$$

with E being the energy and Q_i being the normal mode i. This results in the relevant modes for the VO_4 species as shown in Table 1.3. The accompanying intensities for IR and Raman are also incorporated in this Table. The IR intensities are dependent on the change in dipole moment with the normal coordinate Q_i that is generated by the vibrational mode[43]:

$$\frac{\partial \mu}{\partial Q_i} \quad (1.6)$$

where μ stands for the dipole moment. The intensities of the vibrational modes in Raman are dependent on the change in polarizability[43]:

$$\frac{\partial \alpha}{\partial Q_i} \tag{1.7}$$

where α stands for the polarizabilty. With an assumed standard line broadening of 10 cm^{-1} the theoretical spectra, Figure 1.3, can be drawn and compared with the experimental spectra. As can be seen the intensities for the vibrational modes are different in IR and Raman.

Table 1.3 Vibrational modes calculated for the umbrella model, Figure 1.2D, with the accompanying infrared and Raman intensities.

Vibration	Wavenumber (cm^{-1})	Infrared intensity (km/mole)	Raman intensity (a.u.)
V=O	1038	116	14.2
Si-O-V	978	1823	6.9
O-O	903	324	31.7

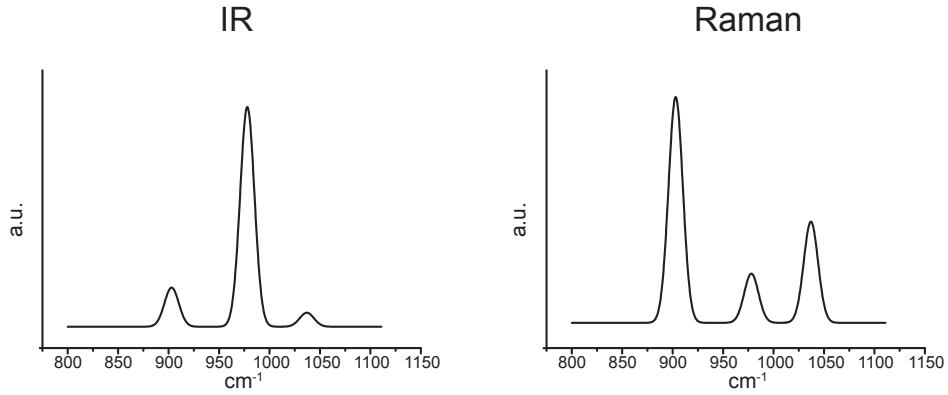

Figure 1.3 Theoretical IR and Raman spectra for the umbrella model, model D in Figure 1.2.

In the same manner the chemical shift of the structure can be calculated as[43]:

$$\frac{\partial^2 E}{\partial B \partial I} \tag{1.8}$$

Where E stands for the Energy, B for the magnetic field and I for the nuclear magnetic moment (nuclear spin). For ^{51}V this can give a shift of roughly 0 - 2000 ppm. Doing this calculation on the umbrella model results in an absolute shift of -2010 ppm or -150 ppm relative to $VOCl_3$.

The same can of course be done for other molecular properties as long as there is an operator for this property. For UV-VIS properties, however, the method of calculation has

to be altered. Single determinant methods, like DFT and HF, are not accurate enough to calculate the excited states which are reached when a photon is absorbed by the model. To do this in a first principle way one should use CI (configuration interaction) methods for this type of molecular properties. However, this is a very time consuming method and cannot sensibly be used for this type of large models. A good approximation is to use the RPA (Random Phase Approximation)[45]. This method takes in account all the single excitations from the ground state. In combination with calculations on reference compounds this method gives a good indication of the onset of the optical absorption. An example of a calculated UV-VIS spectrum is given below in Figure 1.4. The vertical lines in the graph represent the calculated transitions and their oscillator strength. The line gives the calculated absorption spectrum when a line broadening of 0.5 eV is used.

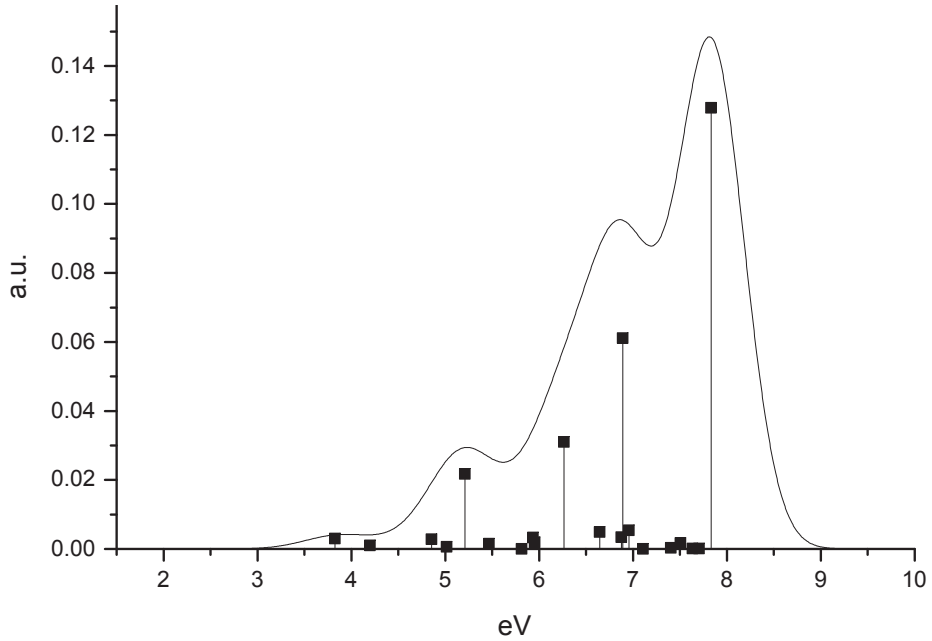

Figure 1.4 Theoretical UV-Vis spectra calculated with RPA for the umbrella model, model D in Figure 2. The spikes represent the calculated absorptions and their oscillator strength. The line spectrum is the sum spectrum with a line broadening of 0.5 eV.

To find possible reaction mechanisms, as discussed in Chapter 5, it is necessary to locate the transition states and all the minima of the possible reaction. These states form a pathway (Figure 1.1) over which a reaction can take place. Transition states are states where the first

derivative of the energy in Eq. 1.3 , the gradient, is zero. In contrast the curvature of one of the second derivatives of the energy, the Hessian, has to be negative, while the rest of them is positive. For example the ABC state in Figure 1.1 is a transition state where the A and C are equally bound to B. Figure 1.5 shows an energy diagram for a possible reaction path for the formation of formaldehyde from methanol. Only stable (non transition) states are shown. In step zero of the reaction the catalyst and the reactants are present. In the next step the methanol adsorbs on the catalysts surface and then decomposes into water and formaldehyde. This cycle repeats itself after which the catalyst is reactivated by the addition of a whole O_2 molecule. In Chapter 5 this diagram will be discussed in more detail.

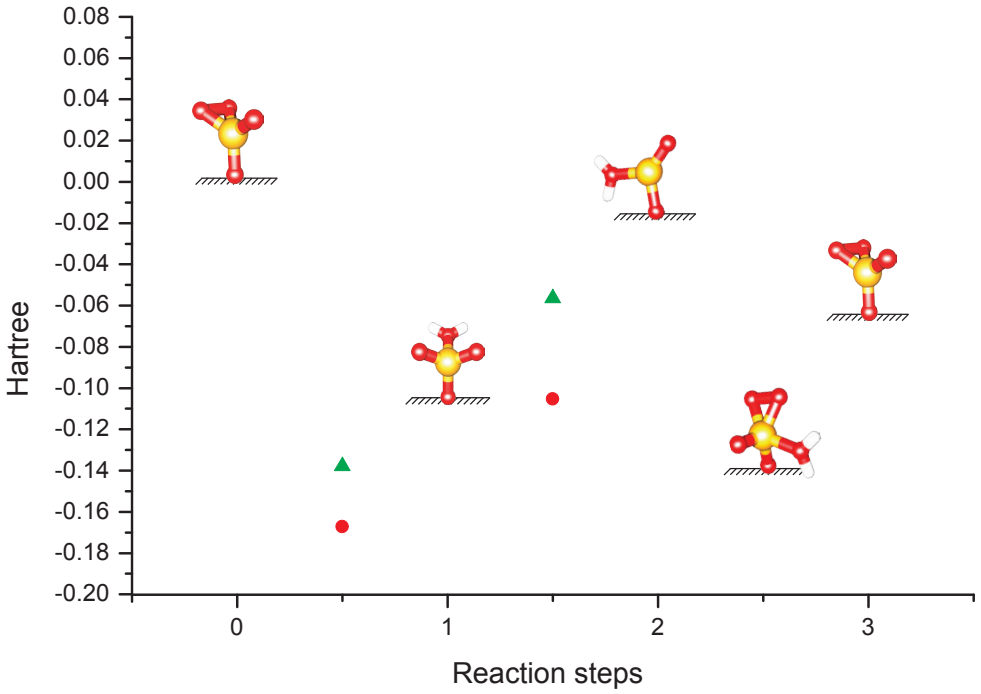

Figure 1.5 Energy diagram for a possible reaction pathway for the formation of formaldehyde over the umbrella model.

References

(1) Hagen, J. *Industrial Catalysis: A practical Approach*; Wiley-VCH: Weinheim, 1999.

(2) Moulijn, J. A.; Leeuwen, P. W. N. M. v.; Santen, R. A. v. *Catalysis an Integrated Approach to Homogeneous, Heterogeneous and Industrial Catalysis*, 2 ed.; Elsevier, Amsterdam, 1993.

(3) Wikipedia; http://www.wikipedia.org.

(4) Chorkendorff, I.; Niemantsverdriet, J. W. *Concepts of Modern Catalysis and Kinetics*; Wiley-VCH: Weinheim, 2003.

(5) Weckhuysen, B. M.; Keller, D. E. *Catal. Today* **2003**, *78*, 25.

(6) Deo, G.; Wachs, I. E. *J. Catal.* **1994**, *146*, 323.

(7) Baerns, M. *Basic Principles in Applied Catalysis*; Springer-Verlag: Berlin, 2004.

(8) Wachs, I. E.; Weckhuysen, B. M. *Appl. Catal. A* **1997**, *157*, 67.

(9) Das, N.; Eckert, H.; Hu, H.; Wachs, I. E.; Walzer, J. F.; Feher, F. J. *J. Phys. Chem.* **1993**, *97*, 8240.

(10) Went, G. T.; Oyama, S. T.; Bell, A. T. *J. Phys. Chem.* **1990**, *94*, 4240.

(11) Bond, G. C.; Könog, P. *J. Catal.* **1982**, *77*, 309.

(12) Bond, G. C.; Sarkany, A. J. *J. Catal.* **1979**, *57*, 476.

(13) Chan, S. S.; Wachs, I. E.; Murrel, L. L.; Wang, L.; Hall, W. K. *J. Phys. Chem.* **1984**, *88*, 5831.

(14) Inomata, M.; Miyamoto, A.; Murakami, Y. *J. Phys. Chem.* **1981**, *85*, 2372.

(15) Iwamoto, M.; Furukawa, H.; Matsukami, K.; Takenaka, T.; Kagawa, S. *J. Am. Chem. Soc.* **1983**, *105,* 3719.

(16) Miyamoto, A.; Yamazaki, Y.; Inomata, M.; Murakami, Y. *J. Phys. Chem.* **1981**, *85*, 2366.

(17) Eckert, H.; Wachs, I. E. *J. Phys. Chem.* **1989**, *93*, 6796.

(18) Kozlowski, R.; Pettifer, R. F.; Thomas, J. M. *J. Phys. Chem.* **1983**, *87*, 5176.

(19) Le Coustumer, L. R.; Taouk, B.; Le Meur, M.; Payen, E.; Guelton, M.; Grimblot, J. *J. Phys. Chem.* **1988**, *92*, 1230.

(20) Wachs, I. E.; Saleh, R. Y.; Chan, S. S.; Cherish, C. C. *Appl. Catal.* **1985**, *15*, 339.

(21) Anpo, M.; Sunamoto, M.; Che, M. *J. Phys. Chem.* **1989**, *4*, 1187.

(22) Deo, G.; Wachs, I. E. *J. Catal.* **1991**, *129*, 307.

(23) Hardcastle, F. D.; Wachs, I. E. *J. Phys. Chem.* **1991**, *95*, 5031.

(24) Ramis, G.; Cristiani, C.; Forzatti, P.; Busca, G. *J. Catal.* **1990**, *124*, 574.

(25) Bond, G. C.; Perez Zurita, J.; Flamerz, S.; Gellings, P. J.; Bosch, H.; Van Ommen, J. G.; Kip, B. J. *Appl. Catal.* **1986**, *22*, 361.

(26) Anpo, M.; Higashimoto, S.; Matsuoka, M.; Zhanpeisov, N.; Shioya, Y.; Dzwigaj, S.; Che, M. *Catal. Today* **2003**, *78*, 211.

(27) Keller, D. E.; de Groot, F. M. F.; Koningsberger, D. C.; Weckhuysen, B. M. *J. Phys. Chem. B* **2005**, *109*, 10223.
(28) Deguns, E. W.; Taha, Z.; Meitzner, G. D.; Scott, S. L. *J. Phys. Chem. B* **2005**, *109*, 5005.
(29) Ferreira, M. L.; Volpe, M. *J. Mol. Catal. A* **2000**, *164*, 281.
(30) Khaliullin, R. Z.; Bell, A. T. *J. Phys. Chem. B* **2002**, *106*, 7832.
(31) Vittadina, A.; Selloni, A. *J. Phys. Chem. B* **2004**, *108*, 7337.
(32) Van der Voort, P.; Baltes, M.; Vansant, E. F. *Catal. Today* **2001**, *68*, 119.
(33) Hohenberg, P.; Kohn, W. *Phys. Rev. B* **1964**, *136*, 864.
(34) Guest, M. F.; Bush, I. J.; van Dam, H. J. J.; Sherwood, P.; Thomas, J. M. H.; van Lenthe, J. H.; Havenith, R. W. A.; Kendrick, J. *Mol. Phys.* **2005**, *103*, 719.
(35) Sayle, D. C.; Catlow, C. R. A.; Perrin, M.-A.; Nortier, P. *J. Phys. Chem.* **1996**, *100*, 8940.
(36) Gijzeman, O. L. J.; van Lingen, J. N. J.; van Lenthe, J. H.; Tinnemans, S. J.; Keller, D. E.; Weckhuysen, B. M. *Chem. Phys. Lett.* **2004**, *397*, 277.
(37) van Lingen, J. N. J.; Gijzeman, O. L. J.; van Lenthe, J. H.; Weckhuysen, B. M. *J. Catal.* **2006**, *239*, 34.
(38) Fock, V. *Z. Physik* **1930**, *61*, 126.
(39) Hartree, D. R. *Proc. Cambridge Phil. Soc.* **1928**, *24*, 89.
(40) Hartree, D. R. *Proc. Cambridge Phil. Soc.* **1928**, *24*, 111.
(41) Stephens, P. J.; Devlin, F. J.; Chabalowski, C. F.; Frisch, M. J. *J. Phys. Chem.* **1994**, 11623.
(42) Hertwig, R. H.; Koch, W. *Chem. Phys. Lett.* **1997**, *268*, 345.
(43) Jensen, F. *Introduction to Computational Chemistry*; Wiley: Chichester, 2001.
(44) E. B. Wilson, J.; Decius, J. C.; Cross, P. C. *Molecular Vibrations; The Theory of Infrared and Raman Vibrational Spectroscopy*; McGraw-Hill Book Company Inc.: New York, Toronto, London, 1955.
(45) Fuchs, C.; Bonacic-Koutecký, V.; Koutecký, J. *J. Chem. Phys.* **1993**, *98*, 3121.

Chapter 2

A new model for the molecular structure of supported vanadium oxide catalysts: the umbrella model

Abstract

The molecular structure of supported vanadium oxide catalysts (VO_4 species) has been investigated, both theoretically and experimentally. Raman scattering experiments were carried out on the temperature dependence of the V=O stretching frequency. The frequency was found to decrease with increasing temperature. Theoretical calculations on the frequencies of several models for the VO_4 species were carried out using density functional theory. It is shown that a consistent description of the data can be obtained if we assume that the VO_4 species are anchored to the oxidic surface by one V-O bond only. The remaining three oxygen atoms point upwards with two equal V-O bonds of 1.79 to 1.80 Å and one shorter bond of 1.59 Å, depending on the details of the cluster model considered. The distance between the support oxygen and the vanadium atom is 1.77 to 1.83 Å.

Based on: Gijzeman, O. L. J.; van Lingen, J. N. J.; van Lenthe, J. H.; Tinnemans, S. J.; Keller, D. E.; Weckhuysen, B. M. Chem. Phys. Lett. 2004, 397, 277. The discussion with respect to a possible $VO(OH)_2$ groups in this paper has been moved to Chapter 4.

2.1 Introduction

Supported vanadium oxide catalysts are widely used in chemical industries in various oxidation reactions as well as for the selective reduction of NO_x with ammonia[1-5]. They consist of a vanadium oxide phase deposited on the surface of an oxide support, such as SiO_2, Al_2O_3, TiO_2 and ZrO_2. During the last two decades many research groups have studied the molecular structure of supported vanadium oxides under hydrated, dehydrated and reduced conditions with e.g. Raman, infrared, UV-VIS and Extended X-ray Absorption Fine Structure (EXAFS) spectroscopies. A review of the literature to date has been published recently[6]. There is a consensus that supported vanadium oxides at low vanadium oxide loadings are present as isolated V centres surrounded by four oxygen atoms.

EXAFS studies performed in our laboratory indicate that a V atom is surrounded by four oxygen atoms, three of these are found at a distance of 1.70 to 1.77 Å, the exact value depending on the nature of the support (alumina, niobia, zirconia) and one at a much shorter distance of 1.58 to 1.59 Å[7]. This suggests, taking into account the presence of an oxidic support a structure like that shown in Figure 2.1, where vanadium is bound to three support oxygens with equal bond lengths. The fourth oxygen atom points upwards, away from the surface and can be described as a double bonded V=O. This model, which might be called the pyramid model, satisfies the two distinct V-O distances found from an analysis of the EXAFS data. The pyramid model predicts the existence of one vibrational mode, which is predominantly the V=O stretch, that should be close to that found in simple V=O structures like VOX_3, with X = F, Cl, Br or I. This mode is indeed reported at around 1030 cm^{-1} by many research groups[8-14].

At higher vanadium oxide loadings the presence of polymeric vanadium oxide species on various supports has been proposed. Experimentally, a second vibrational mode is seen to develop at around 920 cm^{-1} at higher loadings. However, it has also been reported for a 1 wt-% vanadium oxide catalyst on CeO_2[13]. This mode is commonly attributed to a polymeric species, either a V-O-V or an O-V-O bending vibration[14]. However, also a band seen at 1009 cm^{-1} during propane oxidative dehydrogenation[15] has been assigned as due to a polymeric species. On the contrary, a band observed at 1016 cm^{-1} for the partially dehydrated vanadium oxide catalyst has been assigned to a terminal (non-polymeric) V=O bond, as it is seen on a sample with low vanadium loading[8]. Alternatively, the band around 920 cm^{-1} has been assigned to a V-O-Al vibration[10] in studies on a flat Al_2O_3 model catalyst. Thus, the occurrence of many (differently assigned) bands, besides the uncontroversial 1030 cm^{-1} V=O stretching mode, is well documented.

A conventional way to ascertain the assignment of a vibration to a stretching mode is the use of isotopic labelling. For the present case available data are relatively scarce, as it requires the use of ^{18}O. It was found for low loadings of vanadium oxide[6,9] that upon substituting ^{18}O

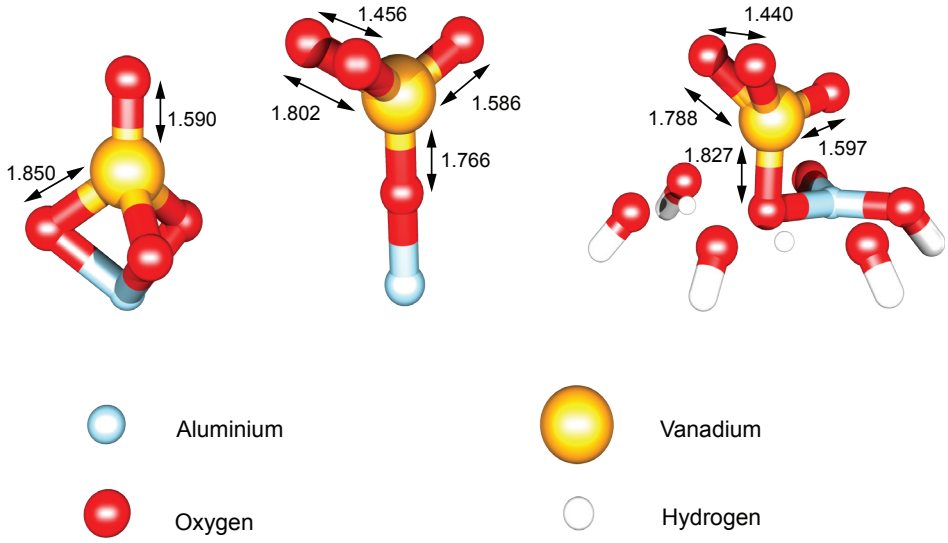

Figure 2.1 The structure of the three cluster models for a supported vanadium oxide (VO_4) catalyst considered in this Chapter. The left hand cluster can be described as a pyramid, with three oxygen atoms forming part of the support lattice. Only one free V=O bond is present, perpendicular to the support surface. The middle and right hand clusters can be described as an umbrella, where only one oxygen atom is part of the support. Two equivalent V-O bonds and one shorter V=O bond are now formed. Bond lengths are indicated in Å.

the 1030 cm^{-1} V=O stretching mode decreased 45 cm^{-1}. This is entirely consistent with the change in frequency for a one-dimensional V=O oscillator. However, the second (polymeric) mode at 920 cm^{-1} also decreases by about the same amount upon substituting labelled oxygen[6,9]. This is somewhat surprising since as a rule bending modes are less susceptible to isotopic substitution.

The terminal V=O mode observed at 1030 cm^{-1} has also been reported to shift to lower wavenumbers with increasing temperature[6,9,15,16], although no explanation for this effect has been proposed. This effect is somewhat surprising, as one would intuitively expect the frequency to increase due to a weakening of the bond between the adsorbate and the surface. For example the CO stretch frequency of the adsorbed molecule is much lower than the gas phase frequency. The effect of temperature on the Raman frequencies of bulk compounds and large crystallites has been noted before[16]. It has been attributed to thermal expansion (anharmonicity) of the lattice.

The controversies and unexplained features of the supported vanadium oxide system led us to reinvestigate this system both experimentally and theoretically. In the present Chap-

ter we wish to propose a completely different molecular structure for the VO_4 moiety also shown in Figure 2.1 as the umbrella model. Here a VO_3 entity is bound to the surface by one V-O bond only. We will show that this model is capable of describing all observed data correctly and consistently.

2.2 Experimental

Supported vanadium oxide catalysts were prepared using Nb_2O_5 (HY-340, CBMM, S_{BET}=190 m^2g^{-1}) and SiO_2 (home made, S_{BET}=600 m^2g^{-1}) as support. The 1 wt-% catalysts were prepared *via* an incipient wetness impregnation of a NH_4VO_3 (Merck, p.a.) solution with oxalic acid (Brocacef, 99.25% pure). The catalysts were dried at room temperature for one night, one night at 120 °C and after that they were calcined at 500 °C for 3 h. This resulted in a series of vanadium oxide catalysts with loadings well below the monolayer coverage.

Raman spectra of supported vanadium oxide catalysts were obtained with the aid of a Kaiser RXN spectrometer equipped with a 532 nm diode laser. A 5.5" non-contact objective was used for beam focusing and collection of scattered radiation. A total of 25 data accumulations was done in an exposure time of 2 s for each datapoint.

Quantum chemical calculations were done with the GAMESS-UK program[17]. The program uses ab-initio methods to solve the non-relativistic Schrödinger equation in the restricted Hartree-Fock case. Harmonic vibrational frequencies can be obtained with the Hessian module, incorporated into the program. From these data the transition moments for the relevant infrared and Raman modes can be found by calculating the transition dipole moment and polarisability derivatives. Adding the electron exchange correlation energy to the calculations was done using the B3LYP density functional[18]. All calculations were performed with a triple zeta basis set augmented with polarisation functions (TZVP) as described previously[19].

Several cluster models were investigated, the pyramid model shown in Figure 2.1 where the support was modelled by three oxygen atoms and one aluminium atom. The umbrella model is also shown in Figure 2.1. The support now consists of one oxygen atom and one aluminium atom only. As this might be a rather simplified representation of an adsorbed molecule, also a larger cluster was considered as shown in Figure 2.1. The support is now represented by a layer of seven close packed co-planar oxygen atoms, the six boundary atoms being terminated with hydrogen atoms. A second layer of atoms, consisting of one aluminium atom and two hydrogen atoms was added as well.

As quantum mechanics deals with energies only and we wish to investigate the effect of temperature on observed vibrational frequencies, we must devise a way to do so. Generally the effect of temperature on a solid is to increase its volume. The interatomic distances are

increased due to the anharmonicity of the lattice vibrations[20,21]. The linear thermal expansion coefficient ($\Delta l/l$) is a quantitative measure of this effect. They are generally in of the order of 1 to $5x10^{-5}$ per degree [20,21], but may be much larger for atoms near the surface. Thermal expansion can be simulated in a quantum chemical calculation for a given solid cluster with an adsorbed molecule by first computing its equilibrium (0 K) structure. Increasing all interatomic distances of the solid cluster simultaneously will then mimic the behaviour of this solid at a non-zero temperature. When adsorption takes place on this solid cluster the adsorbed entities will be allowed to find their optimum geometry, consistent with the underlying solid lattice structure. In order to simulate a truly rigid lattice the solid atoms are assigned a large atomic mass (in our case 1500 amu). This removes all vibrations from the calculated results that originate from the necessarily finite size of the cluster. Thus, referring to Figure 2.1, in the pyramid model we increase (simultaneously) all its interatomic distances and assign a large mass to the three oxygen and one aluminium atom. The adsorbed V=O entity is then allowed the find its equilibrium geometry. For the umbrella models in Figure 2.1 we likewise restrain the position of all atoms except for those of the adsorbed $-VO_3$ moiety.

2.3 Results and discussion

The supported vanadium oxide catalysts show the Raman transition at 1030 cm^{-1} at room temperature. The frequency of this V=O stretch vibration decreases with increasing temperature. Results are shown in Figure 2.2a, for a run where the temperature was decreased stepwise from 600°C to 100°C, followed by two runs with increasing and decreasing temperature. As can be seen the data are very reproducible and show a clear trend. The peak frequency decreases with increasing temperatures by about 10 cm^{-1}. Data below 100 °C are influenced by heating of the sample through the exciting laser beam. This temperature effect has been seen before[9,14-16], albeit in a smaller temperature range.

It is found that for the pyramid model shown in Figure 2.1 that the V=O frequency increases if all internuclear distances of the support were changed simultaneously, simulating the thermal expansion of a solid. Figure 2.2b shows the calculated results for this case. Thus the pyramid model contradicts the experimentally observed frequency decrease in Figure 2.2a. The computed V-O distances, 1.59 Å for the V=O separation and 1.85 Å for the three $V-O_{support}$ distances are close, but not equal to that found in the EXAFS analysis.

We will now consider the results for the umbrella model, essentially one support oxygen atom to which a $-VO_3$ entity is bound by a O-V bond, as shown in Figure 2.1. The support can, in a very simplified form, be described by the addition of one aluminium atom below the surface, which is now composed of one oxygen atom only. This structure has an equilibrium geometry with two equivalent V-O bonds with length 1.80 Å and one shorter bond of

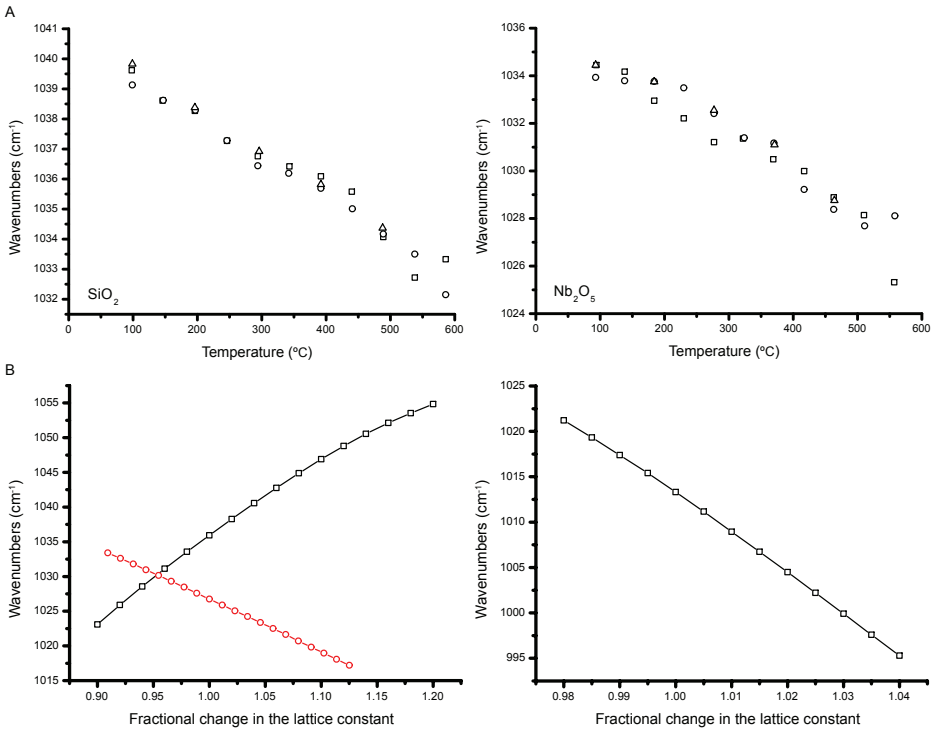

Figure 2.2 A) The temperature dependence of peak maximum of the V=O stretching mode as observed on a silica (left hand side) and niobia (right hand side) supported vanadium oxide catalyst. Three consecutive runs are shown in which the temperature was decreased stepwise from 600 °C to 100 °C (□)*, increased again* (○) *followed by a last cooling down cycle (Δ).*

B) The dependence of the frequency of the V=O stretching mode on the fractional change in the lattice constant of the support lattice for the three models shown in Figure 2.1. The left hand side shown the computed data for the adsorbed -VO_3 species on a small support cluster. An increase in the fractional lattice constant corresponds to a higher temperature due to thermal expansion of the lattice. The pyramidal cluster, with only one oxygen atom pointing away from the surface (□) *shows a temperature dependence, opposite to that found experimentally, whereas the smaller umbrella cluster* (○) *reproduces the experimental trend nicely. The right hand side shows the same data for the large cluster.*

1.59 Å, all pointing away from the surface. The bond between the vanadium and the surface oxygen is 1.77 Å, very close to the distance of the vanadium and the two equivalent oxygens. Similar results were found when adsorbing the -VO_3 entity on the central atom of a plane consisting of seven oxygen atoms in a two-dimensional close-packed structure, with one Al and two H atoms located below this oxygen surface, as also shown in Figure 2.1. Structural

data are given in Figure 2.1 as well for the clusters considered. The umbrella model is thus consistent with the reported EXAFS data on the experimental V-O internuclear distances. It is noteworthy that the molecular structure of the VO_3 contains one V=O bond and two equivalent V-O bonds. The separation between the two equivalent oxygen atoms is only some 1.44 to 1.46 Å, barely larger than that in an oxygen molecule. The structure -VO_3 might thus be described as -$VO(O_2)$, roughly speaking an oxygen molecule adsorbed on a supported V=O species, or a peroxo species.

The harmonic vibrational modes of the two umbrella clusters can be found as well. As is well known the calculated frequencies for DFT wavefunctions are slightly too high, compared with experiments[22]. Commonly a scaling factor around 0.95 is used to correct for this deficiency[23,24]. This factor has been incorporated in all data. Above 800 cm^{-1} two high frequency modes are now found for the small cluster, one at 1027 cm^{-1}, which is predominantly the V=O stretch vibration of the short V-O bond and one at 892 cm^{-1}, which is predominantly the stretching vibration of the two equivalent oxygen atoms. It can be considered as the vibration of a free oxygen molecule (1580 cm^{-1}) weakened by the interaction of this molecule with the V=O entity. The numbers change slightly for the larger cluster (1008, 918 cm^{-1}), but the conclusion holds for both umbrella cluster models.

An increase in temperature can now be simulated by increasing the distance between the aluminium atom and the one surface oxygen atom in the simple cluster or by simultaneously increasing all distances in the larger cluster. It is found that in both cases the two vibrational frequencies decrease with increasing temperature. A plot of the data is shown in Figure 2.2b. Here the x-axis is given as the fractional change in the "lattice constant" of the cluster. For the simple cluster this is just the Al-O distance, the only distance present in the model for the support. For the larger cluster it is the distance between two oxygen atoms in the surface of the cluster, all other distances being scaled proportionally. For this cluster it can be seen from Figure 2.2b that a decrease in the vibrational frequency of around 10 cm^{-1} (as observed experimentally) is caused by a fractional bond length change of 0.014. This implies a linear thermal expansion ($\Delta l/l$) of 0.014. Using an experimental thermal expansion coefficient for bulk solids 1 to $5x10^{-5}$ per degree [20,21] a thermal expansion of 0.005 to 0.025 over a temperature range of 500°C is obtained. This range brackets the computed value nicely. It thus appears that the umbrella model is in agreement with the observed Raman data as well.

The isotopic substitution experiments reported in refs. [10] and [15] can also be included simply by replacing one, two or three oxygen atoms pointing away from the surface by ^{18}O atoms. As can be expected both bands shift to lower wavenumbers if the oxygen atom involved is replaced by its heavier isotope. As the three oxygen atoms pointing upwards from the surface are not equivalent, one (or two) of them can be exchanged in two distinct ways. All possible cases have been considered and the calculated and observed frequencies

are given in Table 2.1 for both clusters considered. The agreement is excellent. Thus the umbrella model is able to explain these observations as well without invoking the presence of polymeric species. This assignment of the 939 cm^{-1} band to the stretching mode of the two equivalent oxygen atoms is further substantiated by the fact that, generally, bending modes are less influenced by isotopic substitution. The bending mode of for instance CO_2 is calculated to shift only some 9 cm^{-1} upon substituting two ^{18}O atoms, whereas the totally symmetric stretch shifts 75 cm^{-1}. Also in water the calculated shift in the stretch vibration is found to be 16 cm^{-1}, compared to 7 cm^{-1} for the predominantly bending modes upon substituting one ^{18}O atom. This also argues against the assignment of the 939 cm^{-1} band as a (polymeric) bending mode.

Table 2.1 Observed and calculated frequencies (cm^{-1}) for partially ^{18}O exchanged O-V-O_3. All possible cases for the exchange of 1, 2 or 3 oxygen atoms have been included.

observed ^{16}O			920		1030
observed $^{18}O/^{16}O$		≈880	920	985	1030
Al-O-V-$^{16}O_3$			892		1027
Al-O-V-$^{16}O_2{}^{18}O$		870			1027
Al-O-V-$^{16}O_2{}^{18}O$			891	985	
Al-O-V-$^{16}O^{18}O_2$		869		985	
Al-O-V-$^{16}O^{18}O_2$	847				1026
Al-O-V-$^{18}O_3$	846			985	
AlH_2O_7-V-$^{16}O_3$			918		1008
AlH_2O_7-V-$^{16}O_2{}^{18}O$		897			1008
AlH_2O_7-V-$^{16}O_2{}^{18}O$			914	971	
AlH_2O_7-V-$^{16}O^{18}O_2$		894		969	
AlH_2O_7-V-$^{16}O^{18}O_2$	873				1008
AlH_2O_7-V-$^{18}O_3$	870			968	

2.4 Conclusions

The following conclusions can be drawn from this work:

(1) The molecular structure of a supported vanadium oxide catalyst can be described as a chemisorbed -V=O(O_2) species. All three oxygen atoms point away from the support surface. Two equal V-O distances are found at 1.79 to 1.80 Å and one shorter V=O bond at 1.59 Å. The equivalent oxygens are separated by only 1.44 to 1.46 Å.

(2) The observed vibrational frequencies in the range 900 to 1130 cm^{-1} can all be assigned to either V=O (1030 cm^{-1}) or O-O (939 cm^{-1}), without invoking the presence of polymeric species.

References

(1) Amiridis, M. D.; Wachs, I. E.; Deo, G.; Jehng, J.-M.; Kim, D. S. *J. Catal.* **1996**, *161*, 247.

(2) Bosch, H.; Janssen, F. J. J. G.; Kerkhof, F. M. G. v. d.; Oldenzieli, J.; Ommeni, J. G. v.; Ross, J. R. N. *Appl. Catal.* **1986**, *25*, 239.

(3) Lopez Nieto, J. M.; Concepcion, P.; Dejoz, A.; Knözinger; Melo, F.; Vazquez, M. I. *J. Catal.* **2000**, *189*, 147.

(4) Wada, K.; Yamada, H.; Watanabe, Y.; Mitsudo, T.-A. *J. Chem. Soc., Faraday Trans.* **1998**, *94*, 1771.

(5) Zhu, Z.; Liu, Z.; Liu, S.; Niu, H. *Appl. Catal. B* **1999**, *23*, 299.

(6) Weckhuysen, B. M.; Keller, D. E. *Catal. Today* **2003**, *78*, 25.

(7) Keller, D. E. *PhD Thesis*, Utrecht University **2006**

(8) Das, N.; Eckert, H.; Hu, H.; Wachs, I. E.; Walzer, J. F.; Feher, F. J. *J. Phys. Chem.* **1993**, *97*, 8240.

(9) Jehng, J., Mirn; Goutam, D.; Weckhuysen, B. M.; Wachs, I. E. *J. Mol. Catal. A* **1996**, *110*, 41.

(10) Magg, N.; Giorgi, J. B.; Schroeder, T.; Bäumer, M.; Freund, H.-J. *J. Phys. Chem. B* **2002**, *106*, 8756

(11) Vuurman, M. A.; Wachs, I. E. *J. Mol. Catal.* **1992**, *77*, 29.

(12) Vuurman, M. A.; Wachs, I. E.; Hirt, A. M. *J. Phys. Chem.* **1991**, *95*, 9928.

(13) Wachs, I. E.; Deo, G.; Vuurman, M. A.; Hu, H.; Kim, D. S.; Jehng, J.-M. *J. Mol. Catal.* **1993**, *82*, 443.

(14) Weckhuysen, B. M.; Jehng, J.-M.; Wachs, I. E. *J. Phys. Chem. B* **2000**, *104*, 7382.

(15) Cortez, G. G.; Bañares, M. A. *J. Catal.* **2002**, *209*, 197.

(16) Xie, S.; Iglesia, E.; Bell, A. T. *J. Phys. Chem. B* **2001**, *105*, 5144.

(17) Guest, M. F.; Bush, I. J.; van Dam, H. J. J.; Sherwood, P.; Thomas, J. M. H.; van Lenthe, J. H.; Havenith, R. W. A.; Kendrick, J. *Mol. Phys.* **2005**, *103*, 719.

(18) Becke, A. D. *J. Chem. Phys.* **1993**, *98*, 5648.

(19) Ahlrichs, R.; Taylor, P. R. *J. Chim. Phys. Phys.-Chim. Biol.* **1981**, *78*, 315.

(20) Ashcroft, N. W.; Mermin, N. D. *Solid State Physics*; Holt, Rinhart and Winston: New York, 1976.

(21) Reissland, J. A. *The Physics of Phonons*; Wiley: New York, 1973.

(22) Dmitrenko, O.; Huang, W.; Polonova, T. E.; Francesconi, L. C.; Wingrave, J. A.; Teplyakov, A. V. *J. Phys. Chem. B* **2003**, *107*, 7747.

(23) Scott, A. P.; Radom, L. *J. Phys. Chem.* **1996**, *100*, 16502.

(24) Wong, M. W. *Chem. Phys. Lett.* **1996**, *256*, 391.

Chapter 3

On the umbrella model for supported vanadium oxide catalysts: A detailed comparison with the classical pyramid model

Abstract

The new model for the molecular structure of supported VO_4 species on alumina, proposed in Chapter 2, has been tested and compared with the classical pyramid model both on a silica support. The model can be described as a chemisorbed $O_{support}$-V=O(O_2) species with a similar geometry as on alumina. Results of DFT calculations on this model are consistent with the experimental Raman and EXAFS data collected on low loaded silica supportedvanadium oxide catalysts. The band observed at 915 cm^{-1} is assigned to an O-O stretch vibration. The thermal motion of the bound O_2 molecule can explain the broadness of this band. This shows that the umbrella model is a viable internally consistent model for supported vanadium oxide catalysts at least at low loadings.

Based on: van Lingen, J. N. J.; Gijzeman, O. L. J.; van Lenthe, J. H.; Weckhuysen, B. M. J. Catal. 2006, 239, 34. The discussion with respect to a possible $VO(OH)_2$ groups in this paper has been moved to Chapter 4.

3.1 Introduction

Supported vanadium oxide catalysts represent an important class of heterogeneous catalysts, which are widely used in chemical industries in various selective oxidation reactions as well as for the selective reduction of NO_x emissions[1-4]. They consist of an active vanadium oxide phase deposited on the surface of a high-surface oxide support, such as SiO_2, Al_2O_3, TiO_2 and ZrO_2. The molecular structure of these supported vanadium oxide species has been studied by a wide variety of spectroscopic techniques, including Raman, ^{51}V NMR, UV-Vis-NIR, EXAFS, XANES, ESR and XPS[5-18]. The reaction rate and selectivity strongly depends on the vanadium oxide loading, support oxide material and degree of hydration. Several review papers can be found in literature, which describes the current understanding of these catalyst systems[5,19-21].

The most common opinion is that the VO_4 monomeric species in dehydrated supported vanadium oxide catalysts can be envisaged as a pyramid structure with one V=O bond and three V-$O_{support}$ bonds (Figure 3.1 d-f)[22-26]. This model is characterized by a vibration at ~1030 cm^{-1} [27]. By comparison with reference compounds this band has been assigned to the V=O stretch vibrational mode[27]. A second rather broad Raman band has been observed at ~915 cm^{-1}, which increases in intensity with increasing vanadium oxide loading, leading to the assignment of this band to polymeric species; i.e., either a V-O-V or an O-V-O vibra-

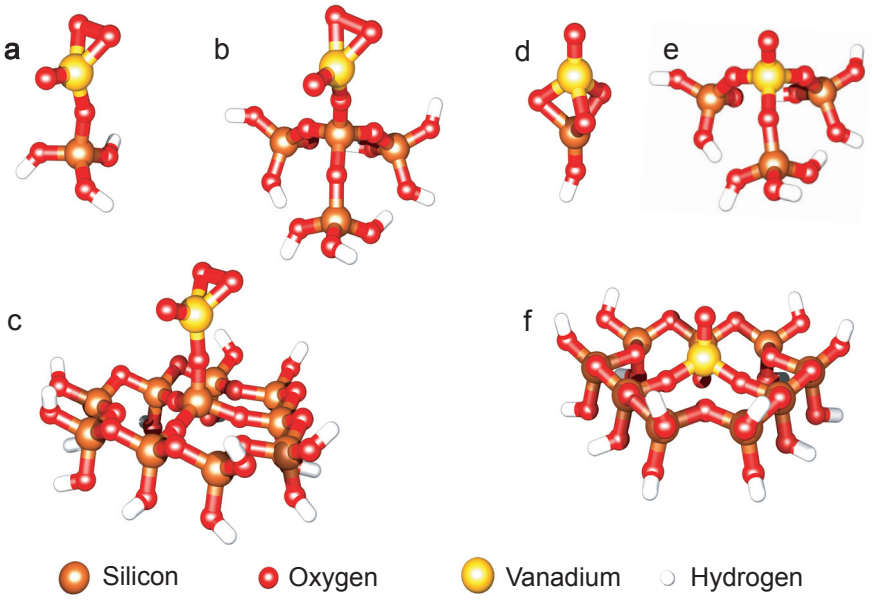

Figure 3.1 The molecular structure of six cluster models (umbrella a-c and pyramid d-f) for a supported vanadium oxide (VO_4) catalyst used for DFT calculations.

tion[16]. Thus, two Raman features are clearly documented in the literature, the 1030 cm^{-1} and 915 cm^{-1} bands. Based on the interpretation given above they have been used as fingerprints to distinguish monomeric and polymeric surface VO_4 units. ^{18}O labeling experiments, in conjunction with Raman spectroscopy[28] provide evidence for this assignment.

Recently, two groups have challenged the assignment of the second band at 915 cm^{-1} to a polymeric vibration. Magg et al.[29] appoint the IR band observed at approximately 915 cm^{-1} for VO_x/Al_2O_3 catalysts to a Al-O-V stretch vibration. We proposed in Chapter 2 an alternative model, nicknamed the umbrella model (Figure 3.1a-c). The VO_4 unit, now containing one V=O unit and an active oxygen "molecule" bound to the vanadium atom, is linked to the surface *via* only one V-O-support bond. This proposal was based on DFT calculations and temperature dependent Raman spectroscopy data on Al_2O_3-supported vanadium oxide catalysts, which could not be explained with the pyramid model. In our current view, the "polymeric" band at 915 cm^{-1} corresponds to an O-O stretching vibration, while the peak at 1030 cm^{-1} still is assigned to a V=O stretch vibration.

In another paper from our group on a VO_x/Al_2O_3 catalyst[30] it was shown with EXAFS that on a low-loaded vanadium oxide catalyst the V atom is surrounded by four oxygen atoms, three of these were present at a distance of 1.72 Å and one at a much shorter distance of 1.58 Å, thus providing support to the "umbrella" or "pyramid" structure. In this article[30], however, it was shown that the V-O-V bonds did not exist, while the 915 cm^{-1} Raman band was observed for this catalyst. Thus, the exclusive assignment of this band to a polymeric species does not seem to be valid.

In this Chapter we will expand our discussion of the umbrella model [31] to the silica support. On this support it has already been shown in the literature[16,27] that the VO_4 species is only monomeric. A series of well-defined VO_x/SiO_2 materials with increasing vanadium oxide loading was prepared and analyzed with EXAFS, Raman spectroscopy and the data were compared to DFT calculations. To sum up we will consider the umbrella and pyramid models by giving an overview of the experimental data that the models are able to explain and commenting on the implications for the reactivity of supported vanadium oxide catalysts.

3.2 Experimental methods

Catalyst preparation

A series of well-defined supported vanadium oxide catalysts with increasing vanadium oxide loading were prepared using SiO_2 (home made, pore volume of 0.70 ml g^{-1} and surface area of 600 m^2g^{-1}) as support oxide. The SiO_2 support was prepared *via* the sol-gel method according to a slightly altered literature recipe[32], i.e. HNO_3 was used instead of HCl. The catalysts were prepared with the incipient wetness impregnation technique using a NH_4VO_3 (Merck, p.a.) solution with oxalic acid (Brocacef, 99.25% pure). The catalysts were dried at

room temperature for 16 h, 16 h at 393 K and after this treatment they were calcined at 773 K for 3 h. In Table 3.1 all catalysts under investigation are listed together with the catalyst code that will be used throughout the paper. The amount of VO_x/nm^2 on the catalysts is compared to the theoretical monolayer for monomers as described by Khodakov *et al.*[33].

Table 3.1 Overview of the supported vanadium oxide catalysts under investigation, together with their corresponding sample code, vanadium oxide loading, surface density and surface monolayer coverage.

Sample	wt% V	VO_x/nm^2	% of monolayer coverage reached
1V-Si	1.05	0.118	5.1
2V-Si	2.08	0.236	10.3
4V-Si	4.05	0.470	20.4
8V-Si	8.33	1.011	43.9
12V-Si	12.90	1.648	71.6
16V-Si	16.40	2.183	94.9

Spectroscopic characterization

Raman measurements were carried out on dehydrated catalyst samples in a special cell with a quartz window. Details on this equipment can be found elsewhere[34]. Dehydration was performed in a stream of O_2 (40 ml min-1) at 723 K for 3 h. Raman spectra (exposure time of 50 s, 50 accumulations) were collected at room temperature with a Kaiser RXN spectrometer equipped with a 532 nm diode laser. A 5.5" non-contact objective was used for beam focusing and collection of scattered radiation.

EXAFS experiments at beamline E4 in Hasylab (Hamburg, Germany) and data analysis were carried out as described previously[30].

DFT calculations

Quantum chemical calculations were done with the GAMESS-UK program[35]. Exchange correlation energy was added to the calculations using the B3LYP density functional[36,37]. All calculations were performed with the LanL2DZ basisset and accompanying ECP's from the EMSL basisset database. The structures of the clusters were optimised to a maximum gradient of 4.4 10^{-5}. After optimizing, harmonic vibrational frequencies were calculated. As is well known the calculated frequencies for DFT wavefunctions are slightly too high, compared with experiments[38]. Commonly a scaling factor of 0.95 is used to correct for this deficiency[39,40]. This factor has been incorporated in all data.

Several cluster models were investigated. In Figure 3.1a the umbrella model presented in Chapter 2 is shown now supported by silica. The support of this cluster consists of one oxygen atom, one silicon atom and three OH-groups only. Larger clusters were considered as shown in Figures 3.1b and c. In the largest cluster the support is modelled by O-$Si_{10}O_{27}H_{15}$, which represents a small part of the amorphous silica support structure. For comparison pyramid model clusters (Figures 3.1d,e, and f) were designed with the same support sizes as used for the umbrella models.

In the vibrational analysis the atoms of the support are assigned a large weight (2000 amu) in order to simulate a truly rigid lattice. This removes all vibrations originating from the support and all couplings between the support and the VO_4 species including a possible V-O-Si vibration. Thus, referring to Figure 3.1a, in case of the smallest umbrella model we assign a huge mass to the Si and OH groups underneath the O-VO_3. This method has been applied to all cluster sizes. In two cases (Figures 3.1b and e) the vibrational frequencies were calculated with the correct weights assigned to the support in order to check the position of the vibrations calculated with the rigidly fixed support . Raman intensities belonging to the vibrations were calculated in the following manner. As GAMESS-UK does not support the calculation of Raman intensities with DFT the intensities were calculated with HF on the HF optimised clusters 1b and 1e in Figure 3.1. Also the H-atoms of the support were frozen to prevent them from having a large influence on the calculated intensities. The vibrations were then linked with the resulting vibrations from the DFT HESSIAN by comparing their movement. The infrared intensities were virtually identical in both cases. Both HF and DFT intensities were calculated with the TZVP basis set[41].

To get an impression of the influence of structural deformation on the vibrational frequencies three possible ways of structural change from the optimal geometry were simulated on the small and medium umbrella models (Figure 3.1b and 3.1c). In all possibilities the geometry was optimised with only the varied parameter fixed, after which the vibrational modes were calculated. Firstly, the VO_3 species of the umbrella model was rotated with respect to the support over a range of 60°. Taking into account the symmetry of the support this rotation covers all positions. Secondly, the Si-O-V bond angle was altered from 120° to 240°. Finally, the distance between the centre of gravity of the bound O_2 molecule and the V atom was changed from 1.5 to 1.8 Å.

The stability of the umbrella and pyramid model relative to each other is difficult to assess since there is no direct comparison possible. We have tried to estimate it by calculation of the reaction energy of the following reactions:

1) $H_3VO_4 + Si(OH)_4 + ½\ O_2 \rightarrow OV\text{-}O_3\text{-}SiOH + 3\ H_2O + ½\ O_2$
2) $H_3VO_4 + Si(OH)_4 + ½\ O_2 \rightarrow O_3V\text{-}O\text{-}Si(OH)_3 + 2\ H_2O$

These reactions start with the same reactants and model the attachment of the vanadium oxide species to the surface. The first reaction yields a pyramid model, the second reaction the umbrella structure. Calculations on this reaction have been performed with the TZVP basis set to get a more accurate result.

3.3 Results

Spectroscopic results

Raman experiments on the VO_4/SiO_2 catalysts after dehydration gave the spectra shown in Figure 3.2. The blank spectrum, taken on only silica, shows three peaks in the 800 till 1200 cm^{-1} region, situated at 800, 980 and 1060 cm^{-1}. These peaks can be assigned to vibrations in the silica lattice. From the spectra with VO_4 present, it can be seen that in the region between 850 cm^{-1} and 1100 cm^{-1} three peaks are visible in the spectra at different loadings: The first extra peak appears immediately at the 1% loading on top of the silica band at 1060 cm^{-1} and becomes more intense with increasing loading. This sharp peak can be assigned to the well-documented V=O stretch vibration at 1040 cm^{-1} [26]. A second sharp peak appears at a loading of 12% and higher. This peak at 996 cm^{-1} is commonly assigned to the formation of crystalline V_2O_5 on the surface[42]. Finally a broad band can be seen at around 915 cm^{-1} at 2% loading and even perhaps at 1% loading. At least the blank sample shows a flat spectrum in that region, while the 1% catalyst shows similar trends as the higher loaded samples. We have previously assigned this band to the O-O stretch vibration of the peroxo group in the umbrella model[31]. Apart from these three peaks the intensity of the broad band at 980 cm^{-1} increases with increasing VO_4 loading, until crystalline V_2O_5 formed from 12V-Si and up.

EXAFS studies[30,43] on the 1V-Si sample resulted in the following structural parameters from the R-space fit: the first shell consists of 1 O-atom at 1.58 Å from the central V-atom. The fitting of the second shell gave 3.07 O-atoms at a distance of 1.77 Å. These results are included in Table 3.2.

DFT calculations

Optimization calculations on the umbrella clusters depicted in Figure 3.1 resulted in 3 structures. The most important distances are shown in Table 3.2. Also included in this table are the calculated vibrational frequencies between 800-1100 cm^{-1}. In Table 3.2 are also included the calculated distances and frequencies for the pyramid clusters (Figures 3.1d-e). Calculating the Hessian with the support atoms at their normal weights i.e. assuming a non-rigid lattice for Figures 3.1b and 3.1e gives a maximum shift in frequency of 2 cm^{-1}.

Distorting the optimal structure of the umbrella model resulted in the graphs shown in Figures 3.3 and 3.4. In these graphs the total energies and frequencies, belonging to the vibrations assigned to the 915 and 1040 cm^{-1} band, are plotted against the structural change.

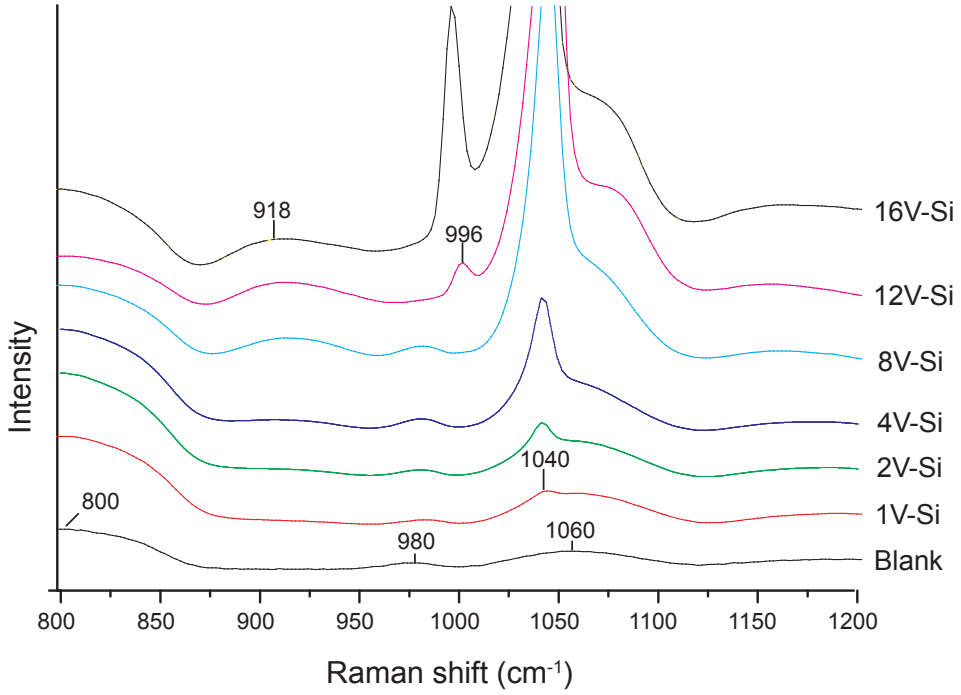

Figure 3.2 Raman spectra of samples (a) 1V-Si; (b) 2V-Si; (c) 4V-Si; (d) 8V-Si; (e) 12V-Si and (f) 16V-Si measured under dehydrated conditions at room temperature. The spectra have been normalised and positioned above each other. For clarity the labels of the spectra have been put to the right of them.

To make a more clear comparison between these three distortions the scales of the graphs have been kept the same. A horizontal line is inserted at the 0.001 hartree level, which is about 1 kT at room temperature. The results for the rotation on the surface of the VO_4 are not shown here, since this distortion had almost no effect on the energy and frequencies of the clusters.

Calculations regarding the stability of the pyramid and the umbrella model resulted in a reaction energy of 262 kJ/mol for the formation of the umbrella species (reaction 2) and 567 kJ/mol for the creation of the pyramid species (reaction 1).

Table 3.2 Computed data with the LanL2DZ ecp basis set for the four umbrella structures combined with the EXAFS and Raman results considered in this work. O_s is the support O-atom. All distances are in Å; vibrational modes are in cm^{-1}. In brackets the coordination number for the atoms at this distance resulting from the EXAFS experiments or the DFT calculations is given.

	Umbrella clusters			Experimental	Pyramid cluster		
	Small (Figure 3.1a)	Medium (Figure 3.1b)	Large (Figure 3.1c)	**EXAFS**	Small (Figure 3.1d)	Medium (Figure 3.1e)	Large (Figure 3.1f)
r(V-O_s)	1.75 (1)	1.75 (1)	1.74 (1)	1.77 (3)	1.83(3)	1.76(3)	1.74(3)
r(V-O)	1.81 (2)	1.80 (2)	1.80 (2)				
r(V=O)	1.59 (1)	1.59 (1)	1.59 (1)	1.59 (1)	1.59(1)	1.59(1)	1.59(1)
r(O-O)	1.54	1.54	1.54	**Raman**			
hν O-O	870	873	867	918	-	-	-
hν V=O	1053	1052	1057	1040	1064	1057	1051
hν Si-O-V	962	980	999	980	647	893	965

3.4 Discussion

EXAFS and DFT studies

The change of the support from alumina, used in the previous Chapter, to silica does not really change the optimized structures for the models as can been seen in Figures 3.1a-f. The umbrella model has one O-atom placed at 1.58 Å, another one at 1.75 Å and two O-atoms at 1.80 Å, which is comparable to the structure on the alumina support. Also it can be concluded from Table 3.2 that these distances do not change significantly when the tiny support (Figure 3.1a) is replaced with one of the larger ones (Figure 3.1b and 3.1c). The size of the silica support is immaterial in the umbrella model.

The pyramid models on almost the same supports as the umbrella models show that when we go to a larger support for this model the $O_{support}$-V distance decreases. This is probably caused by the fact that in the smaller clusters the V-$O_{support}$-Si angles are more strained. They can release this strain by increasing the distances, which will probably cost less energy than straining the angles.

The EXAFS fit results[43] in one O-atom at 1.58 and 3 O-atoms at 1.77 Å from the central V-atom. This compares very well the internal distances (Table 3.1) of the umbrella model if we take into account that EXAFS probably cannot distinguish between 1.75 Å and 1.8 Å, and sees this as three O-atoms at an average of 1.77 Å. The same applies for the pyramid models.

Raman experiments and DFT studies: peak positions and intensities

Raman experiments (Figure 3.2) demonstrate one clear sharp peak at 1040 cm^{-1} and a weak very broad band around 915 cm^{-1}. Next to this the peak at 980 cm^{-1} shows an increase in intensity with increasing vanadium oxide loading. The same features have very recently been observed by Nguyen et al.[44].

DFT Hessian calculations with a Lanl2DZ basis set for the umbrella model [31] clearly show that an O-O stretching vibration of the bound O_2 molecule has a frequency after scaling at 870 cm^{-1} (Table 3.2). This is reasonably close to 915 cm^{-1}. In more time consuming calculations, however, with a TZVP basis set using the same scaling factor, the O-O stretching vibration shifts up by approximately 30 cm^{-1} to the position of around 903 cm^{-1} (Table 3.3). Tables 3.2 and 3.3 also show a Si-O-V vibration found around 980 cm^{-1}. This vibration has a lower intensity in Raman then the other two vibrations, but it is still high enough to be measurable. Its presence explains the increase of intensity of the experimental band at 980 cm^{-1}. The intensity of the Si-O-V vibration in infrared is just the opposite of that in Raman, the 980 cm^{-1} band being the most prominent. It should therefore be the major peak that can be observed experimentally. An example is the work of Scott et al.[45-47], in which an IR band at 959 cm^{-1} is observed and assigned to a Si-O-V vibration, in agreement with our calculations. Possibly the appearance of a peak at 1005 cm^{-1} in IR spectrum of Magg et al.[29]

Table 3.3 Computed relative intensities in infrared and Raman for the most intense vibrational frequencies involving vanadium calculated with the TZVP basis set.

	Vibration	Frequency (cm^{-1})	Intensity infrared (km/mole)	Intensity Raman (a.u.)
Pyramid	V=O	1036	159	2.2
	Antisymm O_3-V=O	1024	903	6.3
	Symm O_3-V=O	1046	72	23.6
	Si-O-V	906	1789	15.8
Umbrella	V=O	1038	116	14.2
	Si-O-V	978	1823	6.9
	O-O	903	324	31.7

can be explained by the intense Si-O-V vibration calculated here. Together with the V=O stretching vibration this gives the three bands at 915, 980 and 1040 cm^{-1}, which are seen in the experimental Raman spectra at low loadings (Figure 3.2).

The calculations done on the pyramid models are able to explain the presence of the V=O vibration at 1036 cm^{-1} in the Raman spectra. A band proposed by Magg et al.[29] to be a V-O-Al mode in the same 900-1000 cm^{-1} region for the pyramid model supported by alumina is calculated around 906 cm^{-1} for a silica supported pyramid as seen in Table 3.3. This vibration is rather an asymmetric VO_3 vibration than a Si-O-V vibration. Table 3.2 shows that the position of this peak really depends on the size of the cluster, ranging from 647 till 965 cm^{-1}. This makes the exact position of this peak doubtful. However, this peak has the largest infrared intensity as can be seen in Table 3.3. In both the experimental infrared spectra from Scott et al.[39,46,47] and Magg et al.[29] it is missing however.

In summary, the umbrella models constructed are able to give a theoretical interpretation for the bands at 915, 980 and 1040 cm^{-1} experimentally observed for silica supported vanadium oxide catalysts by either Raman or IR. The pyramid models are able to explain the band at 1040 cm^{-1} as a V=O vibration and might explain the existence of the 920 cm^{-1} band with the asymmetric O_3-V=O vibration, but fails to give an interpretation for the peak at 980 cm^{-1}.

Raman experiments and DFT studies: band widths

The broadness of the 915 cm^{-1} peak cannot be explained by the first two obvious possibilities, viz. rotation on the surface of the VO_3 umbrella and altering of the Si-O-V bond

angle (Figure 3.3), have almost no influence on the frequencies of the V=O and O-O bands. The third possibility, however, shows that the distance from the O_2 molecule to the V-atom can range from 1.59 to 1.68 Å without increasing the energy of the system by more than 1 kT. This does not affect the frequency of the V=O band, but changes the O-O frequency by 27 cm^{-1}. Thus the change in the position of the bound O_2 molecule caused by thermal energy does indeed lead to a sharp V=O band and a broad O-O band.

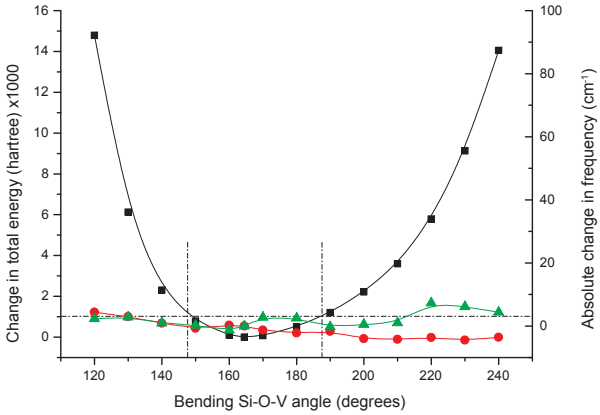

Figure 3.3 The change in energy (total energy - total energy optimized) versus the rotation (■) when the VO_3 species is rotated around the V-O-Si bond; the change in frequency (frequency - optimized frequency) for the 915 cm^{-1} (●) and 1040 cm^{-1} (▲) Raman bands, when the angle of the V-O-Si bond is varied.

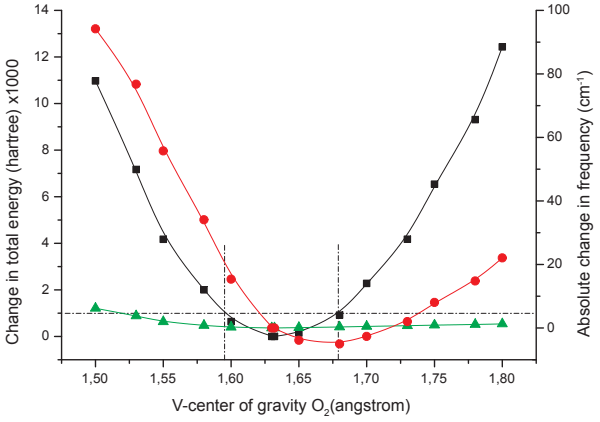

Figure 3.4 The change energy (total energy - total energy optimized) versus the change in distance between the V-atom and the center of gravity of the O_2 molecule (■). The change in frequency (frequency - optimized frequency) for respectively the 915 cm^{-1} (●) and 1040 cm^{-1} (▲) bands with respect to the change in distance between the V-atom and the O_2 molecule.

DFT studies: stability

Concerning the stability of the umbrella model the following things can be said. When we consider the reaction energies of the two reaction equations the formation of the umbrella model (262 kJ/mol) costs half the energy of the formation of the pyramid model (567 kJ/mol). This difference has partially to do with the strains on angles and distances needed to form the pyramid model. In the small pyramid molecule formed in the reaction this will be less then in a real surface. The surrounding atoms on the real surface will be less able to compensate for the strains, thus it will even cost more energy to put it on a surface.

Next to this energy difference, is the fact that OH-groups are rather scarce on the surface. Zhuravlev[48] states that at 300 °C the average area occupied by one OH group on the surface of amorphous silica equals 0.42 nm^2. This makes it very hard to find a surface spot with three OH-groups close enough to form a pyramid active site. The umbrella model only needs one OH-group and can be created everywhere once a hydroxyl group is present on the surface.

The peroxo group is rather tightly bound to the O=V-O_s (-352.3 kJ/mol) from DFT calculations. High temperatures will be needed to remove the bounded O_2 molecule. The oxygen atoms in the O_2 molecule are very reactive and will react with impurities or reactants in the catalytic reaction.

To summarize

If we now consider the umbrella model and combine all the results gathered in this Chapter and Chapter 2 we can say that:

- Both the umbrella and pyramid models comply with the EXAFS studies on VO_4 species supported on either silica or alumina.
- Calculations on the umbrella clusters give three vibrations; the V=O stretch at 1050 cm^{-1}, an Si-O-V mode at 980 cm^{-1} and the O-O stretch in the peroxo group at 870 cm^{-1} (900 cm^{-1} with the TZVP basis set), which can be found in our experimental Raman spectra. The pyramid model cluster have vibrational modes at 1050 (V=O), and 900 cm^{-1} (Si-O-V), but misses a vibration at around 980 cm^{-1}.
- The shift of the 1040 and 920 cm^{-1} peaks by isotope labelling of the O-atoms conducted by Weckhuysen et al.[28] is also reproduced by DFT- calculations.
- The V=O stretch vibration peak is very sharp in the experimental spectra, while the band at 915 cm^{-1} is very broad. This broadness can be explained by the thermal motion of the bound O_2, as shown above.
- The umbrella model gives the same experimentally observed behaviour when the temperature dependence of the peak at 1040 cm^{-1} is simulated on the alumina support. In both the experimental Raman and theoretical calculated data the peak position shifts to a lower frequency with increasing temperature. The same trend can be seen if we

simulate the temperature dependence on a cluster supported by silica. The calculated temperature dependence for the pyramid model gives the opposite trend.

- To form an umbrella structure on the silica surface only one surface OH group is needed. The pyramid model needs three.
- For a similar reaction where a $VOCl_3$ molecule reacts with a silica surface Scott et al.[45-47] found by EXAFS, NMR and several spectroscopic techniques that only one HCl is released per connected $VOCl_3$ unit. This corroborates the umbrella model. They also see an IR peak at 959 cm^{-1}, which they assign to a V-O-Si vibration. Our umbrella model clusters give the same interpretation to this peak position.
- The umbrella model gives more possibilities for a catalytic reaction and makes the reaction scheme simpler. Two O-atoms are readily available for the reaction and one for intermediate H-storage. After all oxygen atoms have been used the catalyst can be reactivated by introducing a new O_2 molecule at the end of the reaction cycle instead. No splitting of an oxygen molecule has to take place as is the case with the pyramid model. This point will be further discussed in Chapter 5.
- Regarding the stability: It takes less energy to form the umbrella model on the surface than it does for the pyramid model. The peroxo group is tightly bound to the $O=V-O_s$ structure, but highly reactive.

3.5 Conclusions

The results presented in this Chapter and the previous one show that the umbrella model is a viable internally consistent model for supported vanadium oxide catalysts at low loadings. The umbrella model can be described as a chemisorbed $-V=O(O_2)$ species. All three oxygen atoms point away from the support surface. Two equal V-O distances are found at 1.79 to 1.80 Å and one shorter V=O bond at 1.59 Å. The equivalent oxygens are separated by only 1.44 to 1.46 Å. The observed vibrational frequencies in the range 900 to 1100 cm^{-1} can be assigned to V=O (1030 cm^{-1}), O-O (915 cm^{-1}) and Si-O-V (980 cm^{-1}), without invoking the presence of polymeric species. Thermal movement of the bound oxygen molecule can explain the broadness of the band at 915 cm^{-1}.

3.6 Acknowledgments

Thanks are due to D.E. Keller for contributing to the experimental data in this Chapter.

References

(1) Gro Nielsen, U.; Topsoe, N.-Y.; Brorson, M.; Skibsted, J.; Jakobsen, H. J. *J. Am. Chem. Soc.* **2004**, *126*, 4926.
(2) Szakacs, S.; Altena, G. J.; Fransen, T.; Van Ommen, J. G.; Ross, J. R. H. *Catal. Today* **1993**, *16*, 237.
(3) Topsoe, N.-Y.; Topsoe, H. *Catal. Today* **1991**, *9*, 77.
(4) Turco, M.; Lisi, L.; Pirone, R.; Ciambelli, P. *Appl. Catal. B* **1994**, *3*, 133.
(5) Weckhuysen, B. M.; Keller, D. E. *Catal. Today* **2003**, *78*, 25.
(6) Wachs, I. E.; Chen, Y.; Jehng, J.-M.; Briand, L. E.; Tanaka, T. *Catal. Today* **2003**, *78*, 13.
(7) Vuurman, M. A.; Wachs, I. E. *J. Mol. Catal.* **1992**, *77*, 29.
(8) Olthof, B.; Khodakov, A.; Bell, A. T.; Iglesia, E. *J. Phys. Chem. B* **2000**, *104*, 1516.
(9) Das, N.; Eckert, H.; Hu, H.; Wachs, I. E.; Walzer, J. F.; Feher, F. J. *J. Phys. Chem.* **1993**, *97*, 8240.
(10) Jhansi Lakshmi, L.; Ju, Z.; Alyea, E. C. *Langmuir* **1999**, *15*, 3521.
(11) Lapina, O. B.; Khabibulin, D. F.; Shubin, A. A.; Bondareva, V. M. *J. Mol. Catal. A* **2000**, *162*, 381.
(12) Deo, G.; Turek, A. M.; Wachs, I. E.; Machej, T.; Haber, J.; Das, N.; Eckert, H.; Hirt, A. M. *Appl. Catal. A* **1992**, *91*, 27.
(13) Tanaka, T.; Yanmashita, H.; Tsuchitani, R.; Funabiki, T.; Yoshida, S. *J. Chem. Soc., Faraday Trans.* **1988**, *84*, 2987.
(14) Haber, J.; Nowak, P.; Serwicka, E. M.; Wachs, I. E. *Bull. Pol. Acad. Sci., Chem.* **2000**, *48*, 337.
(15) Harlin, M. E.; Niemi, V. M.; Krause, A. O. I.; Weckhuysen, B. M. *J. Catal.* **2001**, *203*, 242.
(16) Burcham, L. J.; Deo, G.; Gao, X.; Wachs, I. E. *Top. Catal.* **2000**, *11/12*, 85.
(17) Brückner, A.; Rybarczyk, P.; Kosslick, H.; Wolf, G.-U.; Baerns, M. *Stud. Surf. Sci. Catal.* **2002**, *142*, 1141.
(18) Ruitenbeek, M.; van Dillen, A. J.; de Groot, F. M. F.; Wachs, I. E.; Geus, J. W.; Koningsberger, D. C. *Top. Catal.* **2000**, *10*, 241.
(19) Bond, G. C.; Flamerz-Tahir, S. *Appl. Catal.* **1991**, *71*, 1.
(20) Deo, G.; Wachs, I. E.; Haber, J. *Crit. Rev. Surf. Chem.* **1994**, *4*, 141.
(21) Wachs, I. E.; Weckhuysen, B. M. *Appl. Catal. A* **1997**, *157*, 67.
(22) Wachs, I. E. *Catal. Today* **1996**, *27*, 437.
(23) Takenaka, S.; Tanaka, T.; Yamazaki, T.; Funabiki, T.; Yoshida, S. *J. Phys. Chem. B* **1997**, *101*, 9035.
(24) Oyama, S. T.; Went, G. T.; Lewis, K. B.; Bell, A. T.; Somorjai, G. A. *J. Phys. Chem.*

1989, *93*, 6786.
(25) Eckert, H.; Wachs, I. E. *J. Phys. Chem.* **1989**, *93*, 6796.
(26) Le Coustumer, L. R.; Taouk, B.; Le Meur, M.; Payen, E.; Guelton, M.; Grimblot, J. *J. Phys. Chem.* **1988**, *92*, 1230.
(27) Gao, X.; Bare, S. R.; Weckhuysen, B. M.; Wachs, I. E. *J. Phys. Chem. B* **1998**, *102*, 10842.
(28) Weckhuysen, B. M.; Jehng, J.-M.; Wachs, I. E. *J. Phys. Chem. B* **2000**, *104*, 7382.
(29) Magg, N.; Immaraporn, B.; Giorgi, J. B.; Schroeder, T.; Baumer, M.; Dobler, J.; Wu, Z.; Kondratenko, E.; Cherian, M.; Baerns, M.; Stair, P. C.; Sauer, J.; Freund, H.-J. *J. Catal.* **2004**, *226*, 88.
(30) Keller, D. E.; de Groot, F. M. F.; Koningsberger, D. C.; Weckhuysen, B. M. *J. Phys. Chem. B* **2005**, *109*, 10223.
(31) Gijzeman, O. L. J.; van Lingen, J. N. J.; van Lenthe, J. H.; Tinnemans, S. J.; Keller, D. E.; Weckhuysen, B. M. *Chem. Phys. Lett.* **2004**, *397*, 277.
(32) Weckhuysen, B. M.; de Ridder, L. M.; Schoonheydt, R. A. *J. Phys. Chem.* **1993**, *97*, 4756.
(33) Khodakov, A.; Olthof, B.; Bell, A. T.; Iglesia, E. *J. Catal.* **1999**, *181*, 205.
(34) Weckhuysen, B. M.; Schoonheydt, R. A. *Catal. Today* **1999**, *49*, 441.
(35) Guest, M. F.; Bush, I. J.; van Dam, H. J. J.; Sherwood, P.; Thomas, J. M. H.; van Lenthe, J. H.; Havenith, R. W. A.; Kendrick, J. *Mol. Phys.* **2005**, *103*, 719.
(36) Hertwig, R. H.; Koch, W. *Chem. Phys. Lett.* **1997**, *268*, 345.
(37) Stephens, P. J.; Devlin, F. J.; Chabalowski, C. F.; Frisch, M. J. *J. Phys. Chem.* **1994**, 11623.
(38) Dmitrenko, O.; Huang, W.; Polonova, T. E.; Francesconi, L. C.; Wingrave, J. A.; Teplyakov, A. V. *J. Phys. Chem. B* **2003**, *107*, 7747.
(39) Scott, A. P.; Radom, L. *J. Phys. Chem.* **1996**, *100*, 16502.
(40) Wong, M. W. *Chem. Phys. Lett.* **1996**, *256*, 391.
(41) Ahlrichs, R.; Taylor, P. R. *J. Chim. Phys. Phys.-Chim. Biol.* **1981**, *78*, 315.
(42) Gilson, T. R.; Bizri, O. F.; Cheetham, N. *J. Chem. Soc., Dalton Trans.* **1973**, 291.
(43) Keller, D. E. *PhD Thesis*, Utrecht University **2006**.
(44) Nguyen, L. D.; Loridant, S.; Launay, H.; Pigamo, A.; Dubois, J. L.; Milet, J. M. M. *J. Catal.* **2006**, *237*, 38.
(45) Deguns, E. W.; Taha, Z.; Meitzner, G. D.; Scott, S. L. *J. Phys. Chem. B* **2005**, *109*, 5005.
(46) Rice, G. L.; Scott, S. L. *J. Mol. Catal. A* **1997**, *125*, 73.
(47) Rice, G. L.; Scott, S. L. *Langmuir* **1997**, *13*, 1545.
(48) Zhuravlev, T. *Colloids Surf. A.* **2000**, *173*, 1.

Chapter 4

Determining the molecular structure of supported vanadium oxide Catalysts based on synthesis method and spectral data from theoretical calculations

Abstract

Infrared and Raman spectra have been calculated for several molecular cluster models for supported vanadium oxide catalysts, that are proposed in literature; i.e. the pyramid model, the umbrella model, a model containing two bonds to the support, a V=O group and an OH group and a related model, with one bond to the support, a V=O and two OH groups. From comparison with spectral data from literature it is concluded that two models, the umbrella model and the model with two bonds to the support, are realistic descriptions of the actual catalyst systems. The presence of the particular vanadium oxide species depends on the method of preparation.

4.1 Introduction

Supported vanadium oxide catalysts represent an important class of heterogeneous catalysts, which are widely used in chemical industries in various selective oxidation reactions as well as for the selective reduction of NO_x emissions[1-4]. They consist of an active vanadium oxide phase deposited on the surface of a high-surface oxide support, such as SiO_2, Al_2O_3, TiO_2 and ZrO_2. The molecular structure of these supported vanadium oxide species has been studied by a wide variety of spectroscopic techniques, including Raman, ^{51}V NMR, UV-Vis-NIR, EXAFS, XANES, ESR and XPS[5-18]. Several review papers, which describe the current understanding of these catalytic systems[18-21], can be found in literature.

There is, however, no definite model that can unambiguously explain all the experimental data collected over the years. This may be of no surprise because there are a number of routes to prepare supported vanadium oxide catalysts, each leading to perhaps a different molecular structure of the active species, although a predominant tendency for the pyramid model[22-28] (Figure 4.1A) clearly exists in literature. Table 4.1 illustrates this showing the proposed linkage of the vanadium oxide species to the support in the literature against the synthesis method for vanadium oxide supported by silica to which the discussion of this article will be limited. Table 4.1 illustrates that, besides the pyramid model[22-28] with three V-O_s bonds (where O_s denotes a support oxygen atom), three other models have been proposed

Table 4.1 Structures mentioned in literature for different synthesis methods applied to prepare supported vanadium oxide catalysts.

Synthesis method	Si-O_s-V	(Si-O_s)$_2$-V	(Si-O_s)$_3$-V	Reference
Incipient Wetness Impregnation			x	Wachs et al.[64]
Sol-Gel		x		Hari Prasad Rao et al.[36]
Sol-Gel		x	x	Nguyen et al.[35]
Chemical Vapor Deposition	x	x		Inumaru et al.[31]
Chemical Vapor Deposition	x			Scott et al.[30,32,33]
Chemical Vapor Deposition	x			Van der Voort et al.[34]
Incipient Wetness Impregnation	x			Gijzeman et al.[52,53] Keller[47]

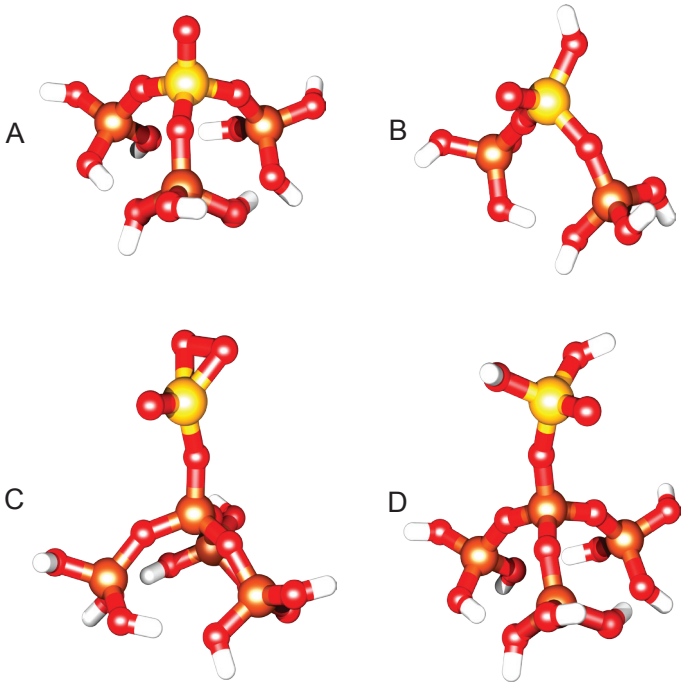

Figure 4.1 The molecular structure of the four cluster models studied in this Chapter:
(A) the pyramid model consisting of a V=O unit bonded to the support with three Si-O_s-V bonds.
(B) a species with two Si-O_s-V support bonds, a V=O and a V-OH group.
(C) the umbrella model with only one support Si-O_s-V bond, a V=O group and a perturbed oxygen molecule bound to the V-atom.
(D) hydrogenated version of the umbrella model where the oxygen molecule is replaced by two OH groups.

as well. Synthesizing the vanadium oxide supported by silica can be roughly divided into two preparation routes: in the first one the support is prepared beforehand, depositing the VO_x species on top by impregnation techniques[29], grafting[30-34] afterwards. This means that the presence of OH groups, during the Si-O-V bond formation (SiOH + VOH → SiOV + H_2O), will be limited by the characteristics of the support, as has been discussed by Inumaru et al.[31]. In the second synthesis route the support oxide is formed at the same time as the VO_x species. This means that in most cases there is an abundance of OH groups. Examples of such routes are the co-condensation of monomeric vanadium $VO_2(OH)_2^-$ and $Si(OC_2H_5)_4$ species in a solution, as recently introduced by Nguyen[35] and the sol-gel synthesis methods[36]. Next to these wet techniques there is a non-chemical preparation of supported VO_x species, which is used by Freund et al.[37-41]. They deposit atomic vanadium on an oxide film under ultra high vacuum (UHV) by means of an electron-beam evaporator.

With these preparation approaches in mind we have looked at the structural models of silica supported vanadium oxide catalysts presented in the last three decades. There is a consensus that the monomeric structure present at low loadings is a distorted tetrahedron around the central vanadium atom and that there are one or more V=O bonds present[26,42-45]. For the incipient wetness technique it has been concluded from EXAFS experiments[46,47] that the V- atom is surrounded by three O-atoms at 1.78 Å and one O-atom at 1.58 Å. The latter should then be related to the presence of a V=O bond. This is as far as the consensus goes. The main difference between the models is the way the tetrahedral VO_4 species is attached to the surface. The pyramid model, introduced in the 1980's, (Figure 4.1A), with three Si-O_s-V bonds connecting it to the surface of the support and a V=O on top is the most popular one[22-28]. Another molecular structure, which has two Si-O_s-V bonds and two V=O bonds, has been presented by Kozlowski et al.[43]. This structure has already been discarded as a viable candidate by Bond et al.[48] and later on by EXAFS experiments[46,47]. The hydrogenated variant of this structure (Figure 4.1B) where one of the V=O bonds is replaced by a V-OH has also been discussed in literature[30,48-51]. In 2004 we have introduced the umbrella model[47,52,53] (Figure 4.1C) where the vanadium atom is linked to the surface *via* only one Si-O_s-V bond and further consists of a V=O and a perturbed O_2 molecule linked to the central vanadium atom. A variation on the umbrella model is obtained when the perturbed O_2 is replaced by two OH groups and has been proposed in 2001 by Van der Voort et al.[34]. This gives a O=V-$(OH)_2$ structure (Figure 4.1D) with still one bond to the support. A related structure emerged, with Cl atoms in place of the OH moieties, in the experiments of Scott et al.[30,32,33] (Figure 4.2).

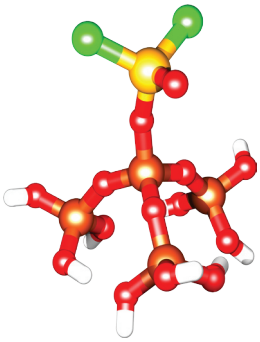

Figure 4.2 The optimized O_s-$VOCl_2$ model of Scott et al.[30,32,33]

In this Chapter theoretical IR and Raman spectra have been calculated with DFT for all the structural models described above supported on a silica support. We compare these theoretical spectra with experimental data found in the literature[33,35,53].

4.2 Experimental methods

The theoretical spectra were calculated with the GAMESS-UK package[54]. All cluster models were optimized to a maximum gradient of 4.4 10^{-5} using the B3LYP density functional[55,56] and the TZVP basis set[57]. After optimizing, harmonic vibrational frequencies and IR intensities were calculated via an analytical Hessian calculation using the same basis. The terminating H atoms were frozen to prevent them having a large influence on the calculated intensities. As is well known the calculated frequencies calculated at the DFT level of theory are slightly too

high, compared with experiments[58]. Commonly a scaling factor of 0.95 is used to correct for this deficiency[59,60]. This factor has been incorporated in all data.

The accompanying Raman intensities were calculated in the following manner. As GAMESS-UK does not currently support the calculation of Raman intensities with DFT, the intensities were calculated at the HF level. The unscaled frequencies differ for HF and DFT so connecting the vibrations was necessary. This was done by visualisation of the vibrations in Molden[61] with the constraints that the calculated HF (scaling factor used for HF was 0.85) and DFT frequencies were within 30 cm^{-1} and the corresponding IR intensities were within 20% of each other. The HF Raman intensity was then assigned to the linked DFT frequency of the vibration. The theoretical spectra have been drawn by giving each vibration the same (10 cm^{-1}) half width. The area underneath the peaks is thus proportional to the calculated intensity of the peak.

Table 4.2 V-O distances found after optimization of the different cluster models in Figures 1 and 2. Distances are represented in Å.

Type of Distance	Pyramid (1A)	$(O_s)_2$-VOOH (1B)	Umbrella (1C)	O_s-$VO(OH)_2$ (1D)	O_s-$VOCl_2$ (2)
V=O	1.578	1.581	1.580	1.577	1.568
V-O	-	1.778	1.799/1.799	1.780	2.170/2.169 (Cl)
V-O_s	1.773 (3x)	1.790/1.757	1.778	1.780/1.780	1.747

4.3 Results

The optimized cluster structures are shown in Figure 4.1. For these clusters the distances from the central V atom to the surrounding O atoms are tabulated in Table 4.2. The calculated vibrations, which include the active species on top of the silica support and their corresponding intensities in IR and Raman are shown in Table 4.3. Figure 4.3 shows the resulting theoretical spectra in Raman and IR respectively in the range from 800 cm^{-1} till 1100 cm^{-1}.

Cluster A (Figure 4.1A), which is the pyramid model[22-28] clearly has two distinguishable IR peaks. One for the asymmetric $(Si\text{-}O_s)_3$-V vibration at 905 cm^{-1} and one asymmetric $(O_s)_3$-V=O at 1024 cm^{-1}. In Raman the band at 905 cm^{-1} remains visible and another peak (symmetric $(O_s)_3$-V=O) at 1045 cm^{-1} becomes dominant. So the most interesting feature here is that the peaks seen in the 1020-1050 cm^{-1} region are in fact highly influenced by the pyramid of O_s atoms underneath it. The pure V=O mode lies in between those peaks, but has a much lower

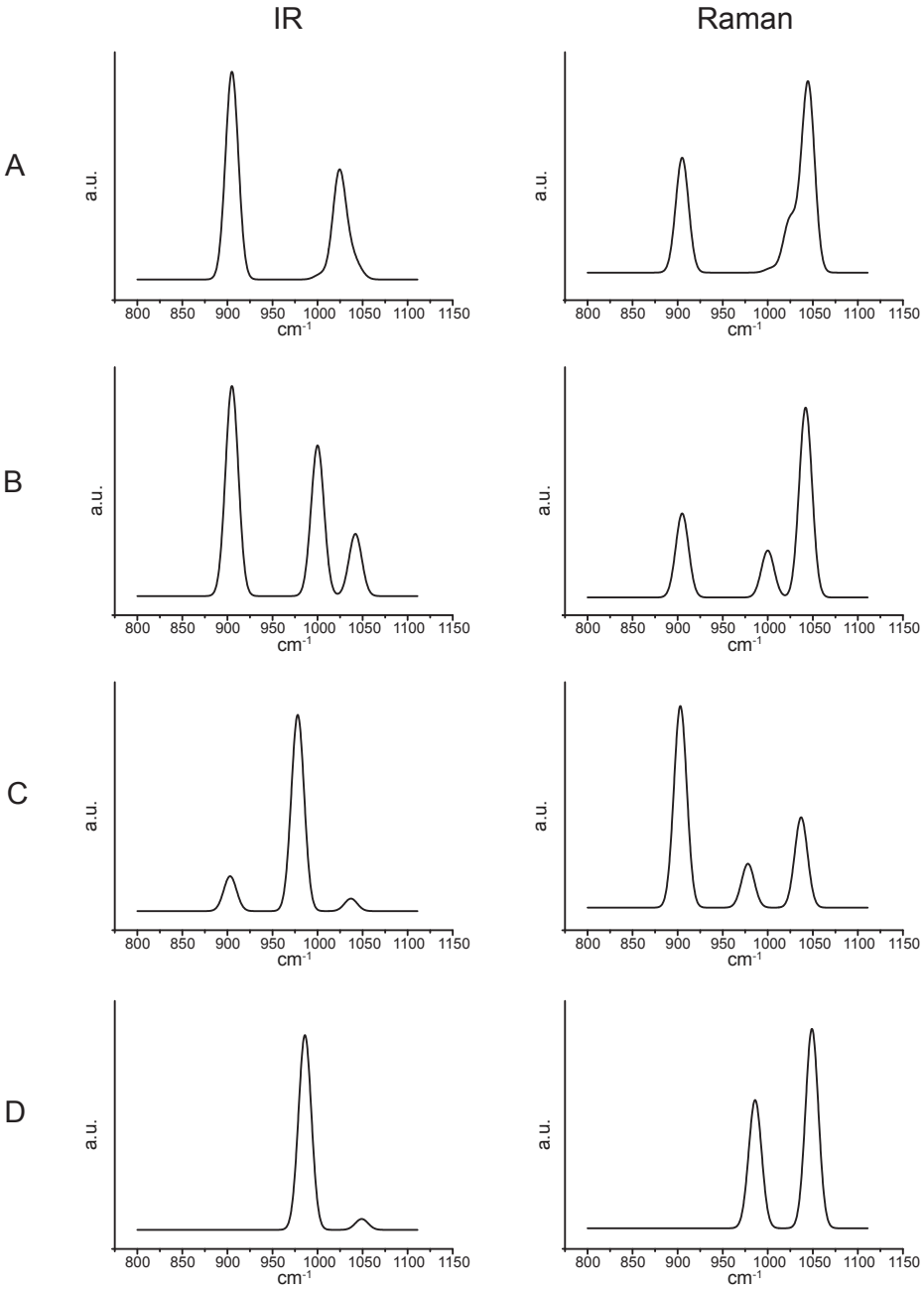

Figure 4.3 Theoretical IR and Raman spectra in the range of 800 1100 cm^{-1} calculated for the clusters shown in Figure 4.1. The letters A-D correspond to the letters next to the models in Figure 4.1.

Table 4.3 Calculated frequencies and intensities in IR and Raman for the active species on top of the support. Per cluster the rows denote frequency, type of vibration, IR intensity (km/mol) and Raman intensity (a.u.) going from top to bottom. The columns have been aligned in such a way that the frequencies (cm^{-1}) of the various clusters are approximately equal. Note that vibrational modes may differ from cluster to cluster.

Pyramid					**905**		**1004**	**1024**	**1036**	**1045**		
Model A					Asym (Si-O_s)3-V		Sym (Si-O_s)$_3$-V	Asym (O_s)$_3$-V=O	V=O	Sym (O_s)$_3$-V=O		
IR					1782		45	903	159	72		
Raman					14.8		0.6	6.3	2.2	23. 6		
O_{s2}-V=O(OH)		**632**		**746**	**905**		**1000**		**1042**		**3658**	
Model B		O-H bend		V-OH stretch	Asym (Si-O_s)$_2$-V		Sym (Si-O_s)$_2$-V		V=O		O-H	
IR		265		219	976		700		289		226	
Raman		3.8		2.3	8.4		4.7		19.0		103	
Umbrella					**903**	**978**			**1037**			
Model C					O-O	Si-O_s-V			V=O			
IR					324	1823			116			
Raman					31.7	6.9			14.2			
O_s-V=O(OH)$_2$	**613**	**635**	**714**	**758**		**986**			**1049**		**3664**	**3368**
Model D	*Asym (O-H)$_2$ bend*	*Sym (O-H)$_2$ bend*	*Sym V-(OH)$_2$ bend*	*Asym V-(OH)$_2$ bend*		Si-O_s-V			V=O		Asym (O-H)$_2$ stretch	*Sym (O-H)$_2$ stretch*
IR	208	281	217	175		1810			101		265	137
Raman	0.0	1.2	7.8	0.7		11.0			17.01		65.4	115.5
O_s-V=OCl_2						**965**			**1046**			
Model E						Si-O_s-V			V=O			
IR						2066			61			

intensity in both IR and Raman. The symmetric $(Si\text{-}O_s)_3$-V vibration at 1004 cm^{-1} has a very low relative intensity in both IR and Raman and will not be visible in experimental spectra.

Cluster B[30,48-51] (Figure 4.1B), with two legs to the support, a V=O group and an OH group, has three peaks in both the IR and Raman spectra between 800 and 1150 cm^{-1}. The first two bands, at 905 cm^{-1} and 1000 cm^{-1}, are related to Si-O_s-V bonds and are more intense in IR than the V=O stretch vibration at 1042 cm^{-1}, which is the most intense in Raman. The OH group gives rise to an O-H stretch vibration at 3658 cm^{-1} and a bend vibration at 630 cm^{-1}. The V-OH stretch, where the hydroxyl group vibrates as a unit lies at 746 cm^{-1}.

The umbrella model (Figure 4.1C) has as discussed before[52,53] an O-O stretch vibration in the perturbed O_2 molecule at 903 cm^{-1}, a Si-O_s-V vibration at 978 cm^{-1} and a V=O stretch vibration at 1037 cm^{-1}. The middle one is the most intense in IR. The first and last are prominent in Raman.

In the hydrogenated version of the umbrella model[34] (Figure 4.1D), four vibrations related to the two OH groups: asymmetric bending 613 cm^{-1}, symmetric bending 635 cm^{-1}, asymmetric stretching 3664 cm^{-1} and symmetric stretching at 3668 cm^{-1} are present. When the hydroxyl groups vibrate as a whole it results in a symmetric and an antisymmetric stretching vibration at 714 and 758 cm^{-1} respectively. In the region of 800-1150 cm^{-1} the V=O at 1049 cm^{-1} and the Si-O_s-V at 986 cm^{-1} are present, although the former is very weak in the IR spectrum.

For the structure presented by Scott et al[30,32,33] (Figure 4.2), the resulting frequencies are presented in Table 4.4.

Table 4.4 IR Frequencies and intensities calculated for the $O_sVO(Cl)_2$ structure introduced by Scott et al.[30,32,33].

	Frequencies (cm^{-1})	Intensities (km/mol)
Symmetric V-Cl_2	425	124
Asymmetric V-Cl_2	474	141
Si-O_s-V	965	2066
V=O	1046	61

4.4 Discussion

V-O Distances

From the V-O distances as presented in Table 4.2 no real distinction can be made between all the cluster models. In all clusters the V=O distances is 1.58 Å. The remaining V-O distances are always 1.78 Å. It does not matter whether those O-atoms belong to the support, the

perturbed oxygen molecule in the umbrella model or the OH groups in clusters B and D. To distinguish between the models is thus impossible with EXAFS when taking in account the first and second coordination shell.

Synthesis, spectra and structure

Route 1: Deposition of the active species upon the already synthesized support

This is the most common way of synthesis, in which the VO_x species is deposited on an already prepared oxidic support[29]. With this technique the X-O_s-V bonds will be formed by elimination of H_2O from one V-OH and one X-OH group. Thus the number and geometry of available hydroxyl groups at the surface determines the number of X-O_s-V bonds. A model with only one surface bond (Figure 4.1C-E) can be formed wherever a surface hydroxyl group is available. For the model (Figure 4.1B) with two surface bonds a distance of about 3 Å between the hydroxyl groups is required for the formation of the Si-O_s-V-O_s-Si unit. For the pyramid model (Figure 4.1A) the hydroxyl groups have to form a triangle with a side of maximum 3 Å on the surface in order to form the cluster. Zhuravlev[62] and Groppo[63] show in their articles that hydroxyl groups are rather scarce on the silica surface and the pictures of a hydrated silica surface drawn by Groppo[63] also show that triangles of hydroxyl groups within a feasible distance of each other are almost non-existing. This means that this method of synthesis has a large chance to generate an active species with only one bond to the surface. This has already been shown experimentally by Scott et al.[30,32,33]. When they deposit $OVCl_3$ on top of a Si-OH group in a silica support only one HCl molecule per adsorbed species is released, which proves that an O_s-$VOCl_2$ structure (Figure 4.2) is formed.

Unfortunately, IR spectra of silica are dominated by intense lattice vibrations at 1050 cm^{-1}. Thus the relevant region of 900 - 1100 cm^{-1} is difficult to study experimentally. The optimal path length through the silica has to be very small in transmission mode as in the case of the experiments conducted by Scott et al.[32,33] Freund et al.[39,41] and Scott et al.[32] show in their IR spectra peaks at 959 cm^{-1} and 1043 cm^{-1}, which were assigned to the Si-O_s-V and a V=O respectively. The calculated spectrum for this O_s-$VOCl_2$ model (Figure 4.2 and Table 4.4) shows a Si-O_s-V vibration at 965 cm^{-1} and the V=O at 1046 cm^{-1}, in good agreement with the assignment of Scott et al.. This confirms their proposed structure and indicates that our calculations are reasonably accurate.

On the contrary an abundance of Raman spectra are available in this region. For clarity we have included the experimental Raman spectra (Figure 4.4) for the dehydrated VO_4/SiO_2 as discussed in Chapter 3. These spectra show the three peaks for the VO_4 species: one clear sharp peak at 1040 cm^{-1} and a weak very broad band around 918 cm^{-1}. In our opinion the peak at 980 cm^{-1} shows an increase in intensity with increasing vanadium oxide loading. So it cannot be completely attributed to the silica support. Thus these three peaks should be

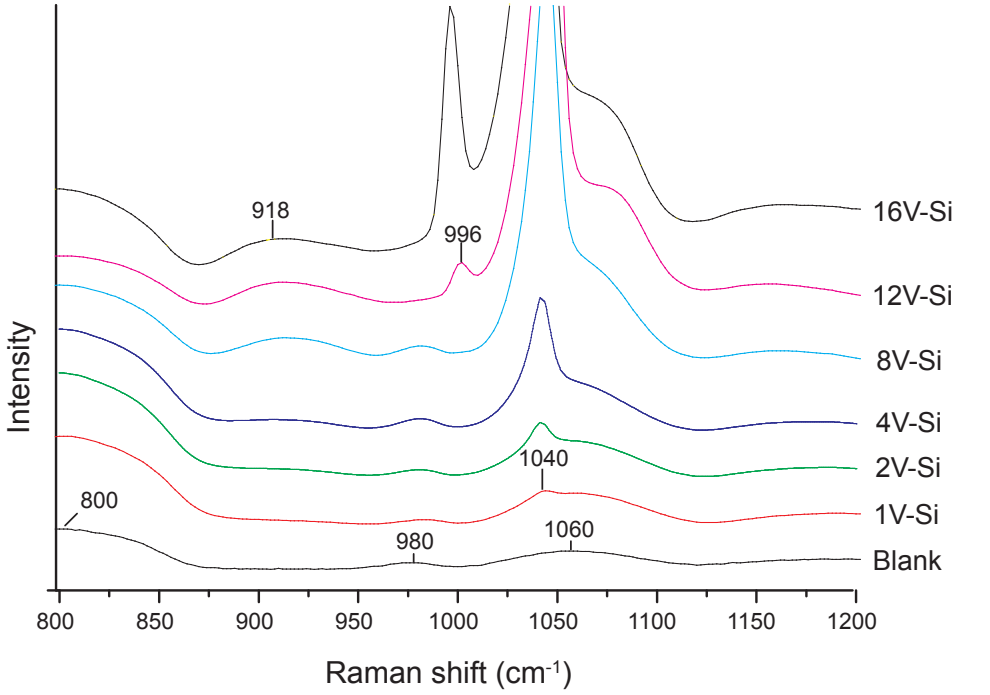

Figure 4.4. Raman spectra of samples (a) 1V-Si; (b) 2V-Si; (c) 4V-Si; (d) 8V-Si; (e) 12V-Si and (f) 16V-Si measured under dehydrated conditions at room temperature. The number before the V in the sample name equals the wt% V. The spectra have been normalised and positioned above each other. For clarity the labels of the spectra have been put to the right of them.

reproduced by our models.

The pyramid model (Figure 4.1A), does not have a peak at around 980 cm^{-1} in contrast to experimental observations (Figure 4.5). The symmetric $(Si\text{-}O_s)_3$-V vibration at 1004 cm^{-1} has a too low intensity in Raman. The asymmetric $(O_s)_3$-V=O band at 1024 cm^{-1} has a Raman intensity that might make it visible as a shoulder on its symmetric counterpart as shown in Figure 4.3A. In order to assign this vibration to the band seen at 980 cm^{-1}, it has to shift downwards for 40 cm^{-1}. After applying the usual correction factor of 0.95, the V=O stretch vibration is calculated almost at the right frequency and it is expected that all three V-O stretch dominated vibrations would shift in the same direction. Therefore, it is highly unlikely that the band seen at 980 cm^{-1} should be assigned to the asymmetric $(O_s)_3$-V=O vibration calculated at 1024 cm^{-1}. The missing peak, the evidence already presented in Chapter 3 and the way of synthesis discard the pyramid model as a suitable model for the result of incipient wetness impregnation.

In the theoretical spectrum of the hydrogenated umbrella model (Figure 4.1D) the peak around 918 cm^{-1} is missing, which is caused by the replacement of the perturbed O_2 molecule by two OH groups. Thus, this model is also not able to explain the experimental observations in Figure 4.4.

This leaves two models to explain the observed spectrum, i.e. the model with two support bonds (Figure 4.1B) and the umbrella model (Figure 4.1C), since they have three peaks visible in roughly the right spectral area. The largest distinction between them is the presence of the OH group in cluster B, which would give rise to an O-H stretch vibration at 3658 cm^{-1}. In the experimental data there was no peak present which could point to an OH group. This favours the umbrella model as the one produced by incipient wetness impregnation.

Route 2: Synthesis of support and active species at the same time

The co-condensation of monomeric vanadium $VO_2(OH)_2^-$ and $Si(OC_2H_5)_4$ at a pH in between 5 and 6 in a solution containing template, was introduced by Nguyen et al.[35]. With this technique the support is generated at the same time as the $VO_2(OH)_2^-$ is deposited. This increases the chance that multiple bonds to the silica precursor are formed from the VO_4 species. Nguyen et al. report in their paper[35] that they suspect that two species are present on the surface; the pyramid model (Figure 4.1A) and the two legged variant with one OH group on top (Figure 4.1B). In their Raman spectrum[35] an intense band is found at 1037 cm^{-1}, which is the V=O stretch vibration. Next to this vibration a very broad band at 920 cm^{-1} is visible. There is also a peak present at 980 cm^{-1} which they attribute to the elongation of the Si-OH groups of the silica support. Comparing these observed frequencies with Table 4.3 leads again to the same conclusion as before in the discussion of the incipient wetness impregnation technique, viz. the umbrella structure is formed on the surface. In contrast to the experimental Raman spectra from incipient wetness impregnation, Nguyen et al.[35] do observe an OH vibration at 3658 cm^{-1}. This is indeed the frequency we calculated for the OH stretch vibration in model B. So the co-condensation preparation method does indeed lead to two distinct vanadium species on the surface, i.e. the umbrella model (Figure 4.1C) and the structure with two support bonds (Figure 4.1B)

Vacuum Deposition

In the preparation of the supported VO_x species which is used by Freund et al.[37-41], first an oxide film is created under UHV. Then atomic vanadium is deposited in an oxygen ambient of 1×10^{-7} mbar by means of an electron-beam evaporator. It is not clear to us what kind of structure for VO_x is to be expected. It will depend on how much O_2 the atomic vanadium picks up before it lands on the surface. Freund et al. conclude that a low temperature (60K) is needed in order to avoid agglomeration[39]. In their STM measurements it is seen that via

diffusion polymeric species are formed at higher temperatures. From this we conclude that the bonds formed with the oxidic surface of the support are weak.

Their IR spectrum for a monolayer coverage only reveals one peak at 1046 cm^{-1}, which is assigned to the V=O vibration. For lower vanadium coverage there is also a band visible at 1005 cm^{-1} shifting to 1035 cm^{-1} and attributed to Si-O_s vibrations. When these IR results are compared with Table 4.3 it is impossible to find a model that fits this spectrum, which is consistent with the findings of Freund et al.[41]. The pyramid model should have a very intense IR band at 905 cm^{-1}. The same applies to the model with two bonds to the support (Figure 4.1B). The umbrella like models have the Si-O_s-V vibration at 978 cm^{-1} which should be very intense in IR. Next to this no OH groups are present which discards models B and D in Figure 4.1.

4.5 Conclusions

It is not possible to make a distinction between our different models for the VO_4 unit by the use of EXAFS when only the first two coordination shells are considered. There are no significant differences between the models regarding the V-O distances. On the basis of experimental and theoretical IR and Raman spectra it can be concluded that for the incipient wetness impregnation techniques[29] the umbrella model (Figure 4.1C) poses a good candidate for the VO_4 species on the surface. The co-condensation technique introduced by Nguyen et al.[35] leads to two structures: Model B (Figure 4.1B) will always be present. Next to this structure the umbrella model (Figure 4.1C) is present. The evaporation of atomic vanadium under UHV on to an oxidic support used by Freund et al.[37-41] gives a structure with such a weak V-substrate interaction, that the geometry of the VO_x unit is unclear to us.

4.6 Acknowledgments

Thanks are due to D.E. Keller for contributing to the experimental data in this Chapter.

References

(1) Gro Nielsen, U.; Topsoe, N.-Y.; Brorson, M.; Skibsted, J.; Jakobsen, H. J. *J. Am. Chem. Soc.* **2004**, *126*, 4926.

(2) Szakacs, S.; Altena, G. J.; Fransen, T.; Van Ommen, J. G.; Ross, J. R. H. *Catal. Today* **1993**, *16*, 237.

(3) Topsoe, N.-Y.; Topsoe, H. *Catal. Today* **1991**, *9*, 77.

(4) Turco, M.; Lisi, L.; Pirone, R.; Ciambelli, P. *Appl. Catal. B* **1994**, *3*, 133.

(5) Brückner, A.; Rybarczyk, P.; Kosslick, H.; Wolf, G.-U.; Baerns, M. *Stud. Surf. Sci. Catal.* **2002**, *142*, 1141.

(6) Burcham, L. J.; Deo, G.; Gao, X.; Wachs, I. E. *Top. Catal.* **2000**, *11/12*, 85.

(7) Das, N.; Eckert, H.; Hu, H.; Wachs, I. E.; Walzer, J. F.; Feher, F. J. *J. Phys. Chem.* **1993**, *97*, 8240.

(8) Deo, G.; Turek, A. M.; Wachs, I. E.; Machej, T.; Haber, J.; Das, N.; Eckert, H.; Hirt, A. M. *Appl. Catal. A* **1992**, *91*, 27.

(9) Haber, J.; Nowak, P.; Serwicka, E. M.; Wachs, I. E. *Bull. Pol. Acad. Sci., Chem.* **2000**, *48*, 337.

(10) Harlin, M. E.; Niemi, V. M.; Krause, A. O. I.; Weckhuysen, B. M. *J. Catal.* **2001**, *203*, 242.

(11) Jhansi Lakshmi, L.; Ju, Z.; Alyea, E. C. *Langmuir* **1999**, *15*, 3521.

(12) Lapina, O. B.; Khabibulin, D. F.; Shubin, A. A.; Bondareva, V. M. *J. Mol. Catal. A* **2000**, *162*, 381.

(13) Olthof, B.; Khodakov, A.; Bell, A. T.; Iglesia, E. *J. Phys. Chem. B* **2000**, *104*, 1516.

(14) Ruitenbeek, M.; van Dillen, A. J.; de Groot, F. M. F.; Wachs, I. E.; Geus, J. W.; Koningsberger, D. C. *Top. Catal.* **2000**, *10*, 241.

(15) Tanaka, T.; Yanmashita, H.; Tsuchitani, R.; Funabiki, T.; Yoshida, S. *J. Chem. Soc., Faraday Trans.* **1988**, *84*, 2987.

(16) Vuurman, M. A.; Wachs, I. E. *J. Mol. Catal.* **1992**, *77*, 29.

(17) Wachs, I. E.; Chen, Y.; Jehng, J.-M.; Briand, L. E.; Tanaka, T. *Catal. Today* **2003**, *78*, 13.

(18) Weckhuysen, B. M.; Keller, D. E. *Catal. Today* **2003**, *78*, 25.

(19) Bond, G. C.; Flamerz-Tahir, S. *Appl. Catal.* **1991**, *71*, 1.

(20) Deo, G.; Wachs, I. E.; Haber, J. *Crit. Rev. Surf. Chem.* **1994**, *4*, 141.

(21) Wachs, I. E.; Weckhuysen, B. M. *Appl. Catal. A* **1997**, *157*, 67.

(22) Anpo, M.; Sunamoto, M.; Che, M. *J. Phys. Chem.* **1989**, *4*, 1187.

(23) Bond, G. C.; Könog, P. *J. Catal.* **1982**, *77*, 309.

(24) Deo, G.; Wachs, I. E. *J. Catal.* **1991**, *129*, 307.

(25) Hardcastle, F. D.; Wachs, I. E. *J. Phys. Chem.* **1991**, *95*, 5031.

(26) Le Coustumer, L. R.; Taouk, B.; Le Meur, M.; Payen, E.; Guelton, M.; Grimblot, J. *J. Phys. Chem.* **1988**, *92*, 1230.
(27) Ramis, G.; Cristiani, C.; Forzatti, P.; Busca, G. *J. Catal.* **1990**, *124*, 574.
(28) Went, G. T.; Oyama, S. T.; Bell, A. T. *J. Phys. Chem.* **1990**, *94*, 4240.
(29) Weckhuysen, B. M.; de Ridder, L. M.; Schoonheydt, R. A. *J. Phys. Chem.* **1993**, *97*, 4756.
(30) Deguns, E. W.; Taha, Z.; Meitzner, G. D.; Scott, S. L. *J. Phys. Chem. B* **2005**, *109*, 5005.
(31) Inumaru, K.; Okuhara, T.; Misono, M. *J. Phys. Chem.* **1991**, *95*, 4826.
(32) Rice, G. L.; Scott, S. L. *J. Mol. Catal. A* **1997**, *125*, 73.
(33) Rice, G. L.; Scott, S. L. *Langmuir* **1997**, *13*, 1545.
(34) Van der Voort, P.; Baltes, M.; Vansant, E. F. *Catal. Today* **2001**, *68*, 119.
(35) Nguyen, L. D.; Loridant, S.; Launay, H.; Pigamo, A.; Dubois, J. L.; Milet, J. M. M. *J. Catal.* **2006**, *237*, 38.
(36) Hari Prasad Rao, P. R.; Ramaswamy, A. V.; Ratnasamy, P. *J. Catal.* **1992**, *137*, 225.
(37) Frank, M.; Bäumer, M.; Kühnemuth, R.; Freund, H.-J. *J. Phys. Chem. B* **2001**, *105*, 8569.
(38) Frank, M.; Kühnemuth, R.; Bäumer, M.; Freund, H.-J. *Surf. Sci.* **2000**, *454-456*, 968.
(39) Immaraporn, B.; Magg, N.; Kaya, S.; Wang, J.; Bäumer, M.; Freund, H.-J. *Chem. Phys. Lett.* **2004**, *392*, 127.
(40) Magg, N.; Giorgi, J. B.; Frank, M. M.; Immaraporn, B.; Schroeder, T.; Bäumer, M.; Freund, H.-J. *J. Am. Chem. Soc.* **2004**, *126*, 3616.
(41) Magg, N.; Immaraporn, B.; Giorgi, J. B.; Schroeder, T.; Baumer, M.; Dobler, J.; Wu, Z.; Kondratenko, E.; Cherian, M.; Baerns, M.; Stair, P. C.; Sauer, J.; Freund, H.-J. *J. Catal.* **2004**, *226*, 88.
(42) Eckert, H.; Wachs, I. E. *J. Phys. Chem.* **1989**, *93*, 6796.
(43) Kozlowski, R.; Pettifer, R. F.; Thomas, J. M. *J. Phys. Chem.* **1983**, *87*, 5176.
(44) Miyamoto, A.; Yamazaki, Y.; Inomata, M.; Murakami, Y. *J. Phys. Chem.* **1981**, *85*, 2366.
(45) Wachs, I. E.; Saleh, R. Y.; Chan, S. S.; Cherish, C. C. *Appl. Catal.* **1985**, *15*, 339.
(46) Anpo, M.; Higashimoto, S.; Matsuoka, M.; Zhanpeisov, N.; Shioya, Y.; Dzwigaj, S.; Che, M. *Catal. Today* **2003**, *78*, 211.
(47) Keller, D. E.; de Groot, F. M. F.; Koningsberger, D. C.; Weckhuysen, B. M. *J. Phys. Chem. B* **2005**, *109*, 10223.
(48) Bond, G. C.; Perez Zurita, J.; Flamerz, S.; Gellings, P. J.; Bosch, H.; Van Ommen, J. G.; Kip, B. J. *Appl. Catal.* **1986**, *22*, 361.

(49) Ferreira, M. L.; Volpe, M. *J. Mol. Catal. A* **2000**, *164*, 281.
(50) Khaliullin, R. Z.; Bell, A. T. *J. Phys. Chem. B* **2002**, *106*, 7832.
(51) Vittadina, A.; Selloni, A. *J. Phys. Chem. B* **2004**, *108*, 7337.
(52) Gijzeman, O. L. J.; van Lingen, J. N. J.; van Lenthe, J. H.; Tinnemans, S. J.; Keller, D. E.; Weckhuysen, B. M. *Chem. Phys. Lett.* **2004**, *397*, 277.
(53) van Lingen, J. N. J.; Gijzeman, O. L. J.; van Lenthe, J. H.; Weckhuysen, B. M. *J. Catal.* **2006**, *239*, 34.
(54) Guest, M. F.; Bush, I. J.; van Dam, H. J. J.; Sherwood, P.; Thomas, J. M. H.; van Lenthe, J. H.; Havenith, R. W. A.; Kendrick, J. *Mol. Phys.* **2005**, *103*, 719.
(55) Hertwig, R. H.; Koch, W. *Chem. Phys. Lett.* **1997**, *268*, 345.
(56) Stephens, P. J.; Devlin, F. J.; Chabalowski, C. F.; Frisch, M. J. *J. Phys. Chem.* **1994**, 11623.
(57) Ahlrichs, R.; Taylor, P. R. *J. Chim. Phys. Phys.-Chim. Biol.* **1981**, *78*, 315.
(58) Dmitrenko, O.; Huang, W.; Polonova, T. E.; Francesconi, L. C.; Wingrave, J. A.; Teplyakov, A. V. *J. Phys. Chem. B* **2003**, *107*, 7747.
(59) Scott, A. P.; Radom, L. *J. Phys. Chem.* **1996**, *100*, 16502.
(60) Wong, M. W. *Chem. Phys. Lett.* **1996**, *256*, 391.
(61) Schaftenaar, G.; Noordik, J. H. *J. Comp.-Aided Mol. Design* **2000**, *14*, 123.
(62) Zhuravlev, T. *Colloids Surf. A.* **2000**, *173*, 1.
(63) Groppo, E.; Lamberti, C.; Bordiga, S.; Spoto, G.; Zecchina, A. *Chem. Rev.* **2005**, *105*, 115.
(64) Wachs, I. E. *Catal. Today* **1996**, *27*, 437.

Chapter 5

Towards a mechanism for the selective oxidation of methanol over supported monomeric vanadium oxide catalysts

5.1 Introduction

Supported vanadium oxide catalysts are widely used in chemical industries in various oxidation reactions as well as for the selective reduction of NO_x with ammonia[1-5]. They consist of a vanadium oxide phase deposited on the surface of an oxide support, such as SiO_2, Al_2O_3, TiO_2 and ZrO_2. During the last two decades many research groups have studied the molecular structure of supported vanadium oxides. A review of the literature to date has been published recently[6]. In previous work, we have proposed a new model for the molecular structure of vanadium oxide catalysts[7,8]. It was shown that the structure could be described as a VO_4 entity, where the V is bound to one support oxygen atom only. The remaining three oxygen atoms point upwards, away from the surface. One of these is found at a distance of 1.60 Å and forms essentially a V=O double bond. The other two are found at the same (larger) V-O distance of 1.80 Å. The separation between the latter two oxygen atoms is only some 1.45 Å. Thus, the structure might be described as $O=V(O_2)$, or an adsorbed oxygen molecule on a V=O unit. This structure is consistent with observed experimental EXAFS and Raman data on the catalyst and has three vibrational transitions, at 1038, 978 and 903 cm^{-1}, which have indeed been observed[8].

The supported vanadium oxide catalyst is known to catalyze selective oxidation reactions such as the conversion of propane to propene[9,10] and the conversion of methanol to formaldehyde[11-13]. Theoretical studies on these reactions mechanisms based on the classical pyramid model have been published before[13-15]. In the present Chapter we want to investigate whether the umbrella model is capable of rationalizing the action of supported vanadium oxides as a selective oxidation catalyst. In this Chapter we only consider the selective oxidation of methanol to formaldehyde:

$$2\,CH_3OH + O_2 \rightarrow 2\,CH_2O + 2\,H_2O \qquad (5.1)$$

A possible route is depicted in Figure 5.1. With the three readily available oxygen atoms present, the selective oxidation occurs twice before the catalyst has to be reactivated by the addition of a whole oxygen molecule. Both steps remove one oxygen atom. Note that a change in multiplicity occurs in the last reaction step, where an oxygen molecule must go from a triplet to a singlet state. Oxygen atoms from the support do not play an active role in this reaction and therefore we will describe the active species as $-VO(O_2)$, where the "-" denotes the bond between the vanadium atom and the oxygen support atom. The basic species in the reaction are then: the initial $-VO(O_2)$ species, a $-VO(O)$ species and a -VO species, as shown in Figure 5.1. The steps in between these species, the actual conversion of methanol into formaldehyde and water can take place on one or two available oxygen atoms from the $-VO_3$. Thus the first step in Figure 5.1 can take place via two different routes given in Figures 5.2a and 5.2b.

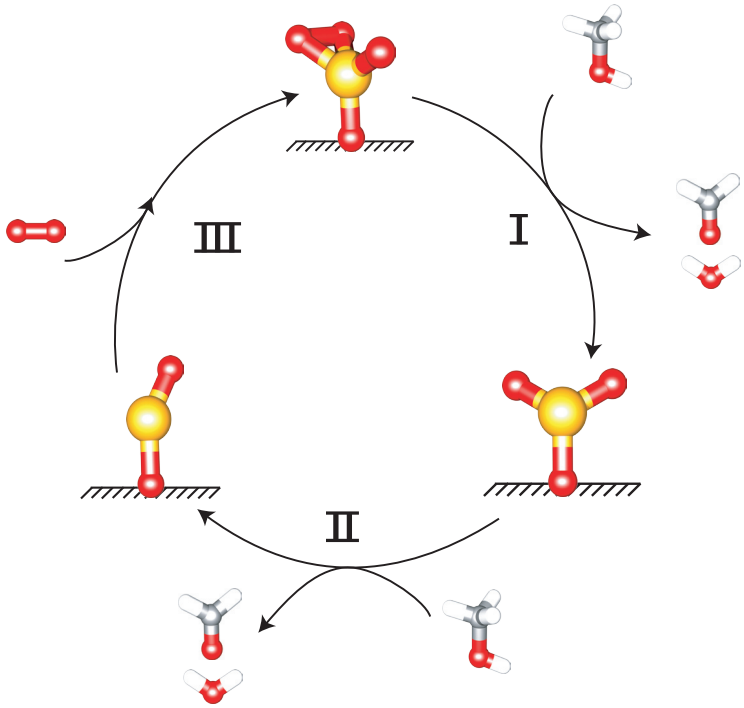

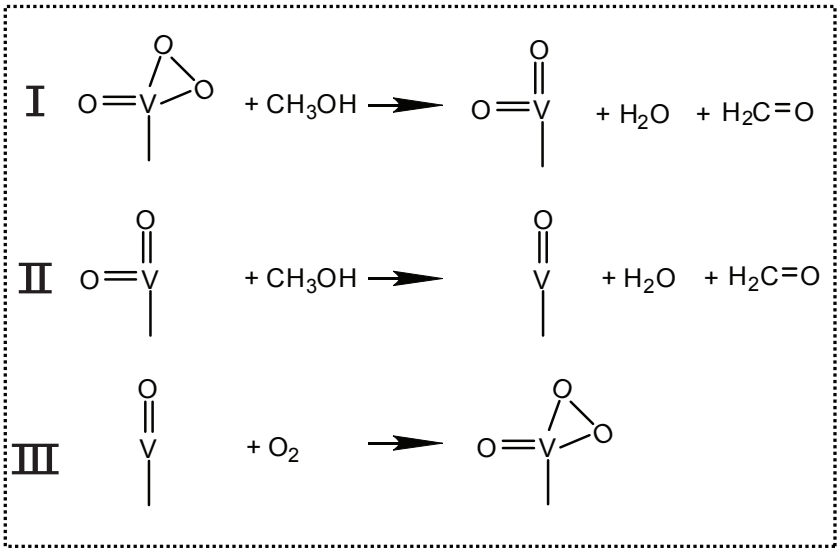

Figure 5.1 Reaction cycle for the selective oxidation of methanol to formaldehyde based on the umbrella model.

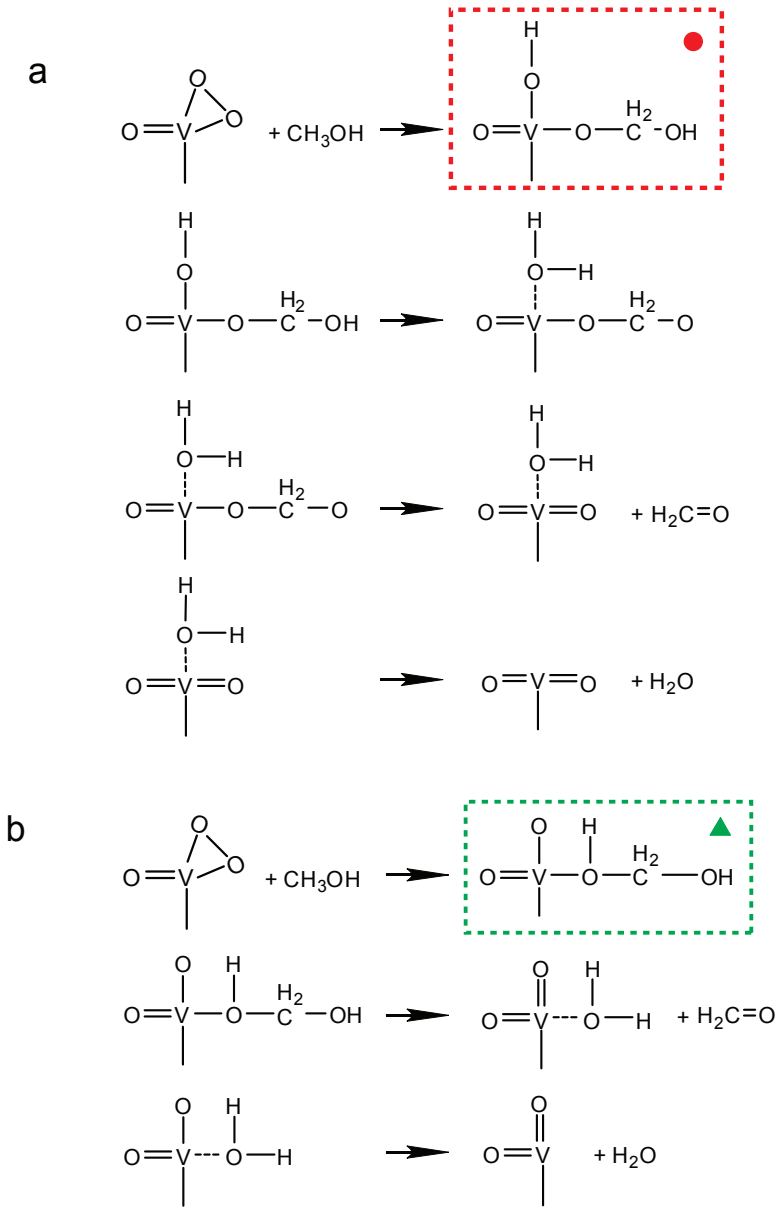

Figure 5.2 Possible route for the first reaction cycle in Figure 5.1. The marked species are also depicted in Figure 5.4.

In the first route (Figure 5.2a) the reaction takes place on two oxygen atoms of the -VO_3 species. The alternative route uses only one oxygen atom from the -VO_3 species. After either of these routes one formaldehyde and one water molecule have been formed.

A question that has to be answered is what happens with the water produced; does it interact with the catalyst? The catalyst can be described as -VOO or -VOO(OH_2), if the water produced remains bound to the vanadium atom. The former case is drawn in Figure 5.1. Starting from the -VOO entity, the second step produces a (second) formaldehyde molecule plus water following the same alternative routes in Figure 5.2, where one oxygen (bound to the vanadium) is absent. Now the active center can be described as -V=O, -VO(OH_2) or -VO(OH_2)$_2$ depending on the binding energy of water. The first possibility is sketched in Figure 5.1. Regeneration of the catalyst can then be accomplished by the addition of one oxygen molecule, step 3 in Figure 5.1.

In the following we give an overview of all the reaction intermediates and we will show that it results in a reasonable reaction mechanism, which explains experimental data in the literature to be discussed later.

5.2 Methods

Quantum chemical calculations were done with the GAMESS-UK program[16]. Exchange correlation energy was added to the calculations using the B3LYP density functional[17,18]. All calculations were performed with the LanL2DZ basis set and accompanying ECP's. The structures of the clusters were optimised to a maximum gradient of 4.4 10^{-5}. After optimizing, harmonic vibrational frequencies were calculated. As is well known the calculated frequencies for DFT wavefunctions are slightly too high, compared with experiments[19]. Commonly a scaling factor of 0.95 is used to correct for this deficiency[20,21]. This factor has been incorporated in all data. The H-atoms of the support were frozen to prevent them from having a large influence on the calculated intensities.

Two cluster sizes were tested to model the SiO_2 support for the vanadium catalyst. In the simplest cluster, the support is modeled by three OH-groups connected to the central silicon atom. A more extensive cluster can be formed by addition of three O-Si(OH)$_3$ units to the central silicon. The umbrella model is shown in Figure 5.3 with the different supports. Table 5.1 gives the results for the interatomic distances and the V=O and V-O vibrational frequencies for the two clusters sizes considered.

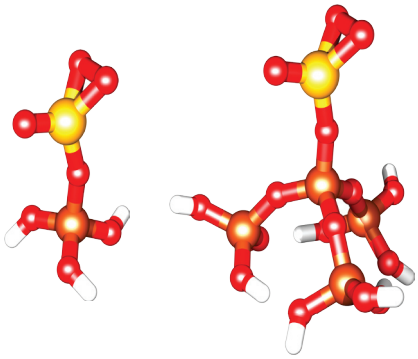

Figure 5.3 The different support clusters tested for the umbrella model.

Table 5.1 Comparison between the small ($Si(OH)_3$) and the larger ($Si(OSi(OH_3)_3$) support in distances, vibrations and energy.

	$-VO_3$		**$-VO_2$**		**-VO**	
support	small	large	small	large	small	large
distances						
V-O_s	1.750	1.754	1.765	1.775	1.828	1.846
V-O	1.806	1.803				
V-O	1.806	1.803	1.608	1.605		
V=O	1.590	1.589	1.608	1.605	1.611	1.610
vibrations						
ν V=O	1110.24	1107.83	1055/1076	1058/1080	1064	1066
ν Si-O-V	1047.3	1075.52	1074.800	1076.83	1047	1058
ν O-O	918.1	918.98				
Energy difference	0	0	75.1545	75.1541	150.4459	150.4423

The results are essentially identical as we also have shown in Chapter 3. Also the energy differences between the clusters with a simple and a more extensive support are the same. The most relevant feature for the catalysis is the $-VO_3$ moiety, which is a rather isolated species and not really affected by the support apart from detailed energetics. For ease of computation we will use the smallest cluster in the remainder of this Chapter. It can be seen from Table 5.1 that as long as the V atom is bound to at least one free oxygen atom this bond will be short (1.6 Å) and will give rise to a V=O stretch mode in the 1000 - 1055 cm^{-1} region.

For comparison of the total energies the energy of the reactants (methanol and oxygen) and products (formaldehyde and water) has to be calculated using the same basis set. The energies that were found were then summed to obtain the total energy in each stage of the reaction.

Strictly speaking we should consider changes in Gibbs free energy (ΔG) to see whether a process takes place spontaneously. This involves a calculation of both ΔH and ΔS for the process considered. ΔH can be simply obtained for ideal gasses as:

$$\Delta H = \Delta E + \Delta(PV) = \Delta E + kT\Delta n \tag{5.2}$$

Where Δn is the change in the number of gas phase molecules. ΔS, also needed for ΔG, can be obtained from knowledge of the translational , vibrational and rotational partition functions, if the pressure of all compounds (reactants and products) is known. As experiments are usually done on systems not in thermodynamic equilibrium, the pressures of the products are unknown. As ΔG is given by:

$$\Delta G = \Delta H - T\Delta S = \Delta E + kT\Delta n - T\Delta S \tag{5.3}$$

its computation involves a guess for ΔS, which is not very accurate. In the following we will use the rule of thumb that entropy is increased if the number of product gas phase molecules increases due to the reaction[22]. Thus the actual free energy differences will be smaller than the corresponding, here reported, energy differences in this case.

5.3 Results and Discussion

Table 5.2 gives the total energy (intermediate cluster + gas phase molecules) for all steps in the conversion of methanol in formaldehyde and water. Figure 5.4 illustrates these in an energy diagram.

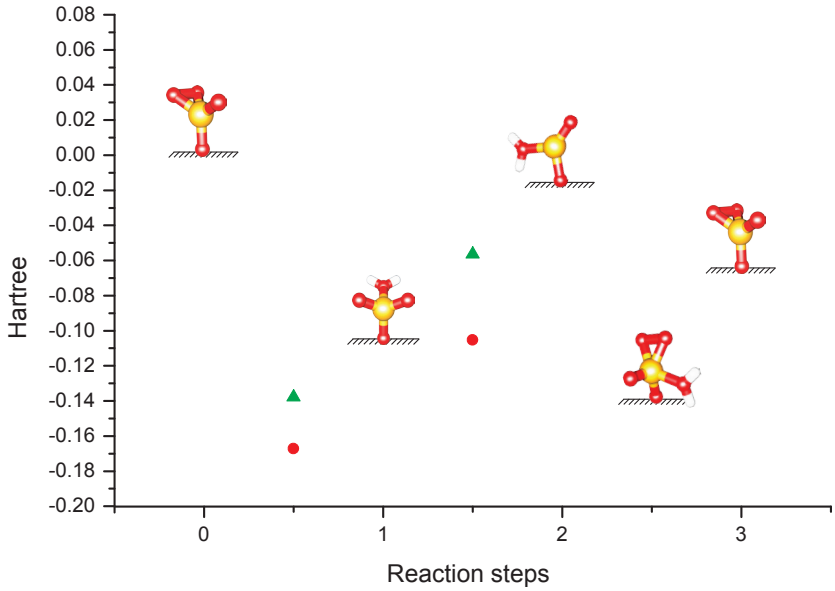

Figure 5.4 Energy diagram for the complete reaction pathway including stable intermediates. De energy indicated includes the energies of the molecules in the gas phase. Dots mark the energy for the intermediate shown in Figure 5.2a. The triangles indicate the energies for the intermediate of Figure 5.2b.

Table 5.2 Characteristic relative energy, V=O distance and vibration frequencies for the steps in the reaction mechanism in Figure 5.4.

step	structure	In gas phase	energy	V=O (Å)	V=O vibration (cm^{-1})
0	$-VO_3$	$2\ CH_3OH + O_2$	0	1.590	1055
0.5a	$-VO(OH)(OCH_2OH)$	$CH_3OH + O_2$	-0.16731	1.598	1035
0.5b	$-VO(O)(OHCH_2OH)$		-0.13831	1.610/1.631*	1017 /966*
1	$-VO_2(OH_2)$	$CH_3OH + CH_2O + O_2$	-0.10681	1.616/1.613	1020(anti)/ 997(sym)
1.5a	$-VOH(OH_2)(OCH_2OH)$	$CH_2O + O_2$	-0.10531	-	-
1.5b	$-VO(OH_2)(OHCH_2OH)$		-0.05641	1.65289*	929*
2	$-VO(OH_2)$	$2\ CH_2O + H_2O + O_2$	-0.01698	1.60963	1018
2.5	$-VO(OH_2)(O_2)$	$2\ CH_2O + H_2O$	-0.14021	1.59315	1039
3	$-VO_3$	$2\ CH_2O + 2\ H_2O$	-0.06591	1.590	1055

*hydrogen bond to the adsorbed methanol

Reaction intermediates in the first cycle, steps 0 to 1

Figure 5.2 gives two possible routes, "a" and "b", for this first step, using two different intermediates; $-VO(OH)(OCH_3OH)$ or $-VO(O)(OHCH_2OH)$. The total energies for these intermediates are given in Table 5.2 and shown in Figure 5.4. Both lie well below the initial energy of the reactants, -0.16731 and -0.13791 a.u. (-439 and -362 kJ/mol), respectively. So option "a" is a little more favored, however it needs to attach the methanol to two oxygen atoms of the $-VO_3$ species, while option "b" only needs one oxygen.

Water

As water is released in this first step it may remain on the catalyst, bound to the vanadium atom via VanderWaals interactions, leaving one molecule of water at the $-VO_2$ unit, as formed after the reaction of one methanol molecule (the first step in Figure 5.1) leads to an energy lowering of 0.084 a.u. (220 kJ/mol). This suggests that the intermediate is stable under reaction conditions (230-360°C [23]). The presence of one H_2O on the $-VO_2$ structure

is included in Fig 5.4.

Reaction intermediates for the second cycle, steps 1 to 2

The second step starts with a water attached, -VO(O)(OH_2). Again the intermediates shown in Figure 5.2 can be formed, however this time the extra water remains attached during the whole process. This time the steps in Figure 5.2a are more difficult to accomplish since the active oxygen atoms left on the vanadium, that are both needed, are almost opposite of each other. Thus this route is less likely. However, both routes lead to the formation of one formaldehyde and one water molecule. This second water molecule produced could also stay attached to the vanadium. Adding one water molecule to the -VO entity leads to an energy lowering of 0.076 a.u. (200 kJ/mol), adding the second water molecule releases only 0.036 a.u. (95 kJ/mol). Thus, the second water molecule is less tightly bound and should be absent under reaction conditions. The stability of the absorbed water molecule is in agreement with the experimental observation that high temperatures (500°C) are needed to dehydrate the sample[24,25]. After these two steps the catalyst has produced two molecules of formaldehyde and two molecules of water, one of which stays attached to the -V=O unit as -V=O(OH_2), see Figure 5.4.

Regeneration

The last step in the reaction mechanism is the regeneration of the catalyst by the attachment of a oxygen molecule to the -VO(OH_2) species and a change in spin multiplicity. This results in the intermediate -VO(OH_2)(O_2). The binding energy of the water molecule is 0.074 a.u. (194 kJ/mol), which means that it not easily removed to get a real regeneration of the catalyst. However, the binding energy of the oxygen molecule is 0.123 a.u. (323 kJ/mol) and is almost twice the strength of the water molecule. Since during the reaction oxygen is abundantly available and water is not, energy favors the replacement of a water molecule by an oxygen molecule.

A new look on reaction mechanism experiments

Table 5.2 gives also the V=O distances and vibrational frequency for all intermediates. During the reaction cycles the frequency decreases gradually with every step in the reaction only to increase again during the regeneration of the catalyst. The question is whether this is visible in experiments.

The species -VO(OH)(OCH_2OH) or -VO(O)($OHCH_2OH$) are the most stable intermediates in Figure 5.4. So their presence might by observed experimentally. All have a weakened V=O vibration at a slightly lower frequency (see Table 5.2). The clusters -VO(O)($OHCH_2OH$) and -VO(OH_2)($OHCH_2OH$) have a really low frequency for the

V=O stretch vibration, this is caused by interference of a hydrogen bond formed between the OH group of the adsorbed methanol and the actual V=O group.

The paper by Burcham et al.[23] presents Raman spectra of a vanadium catalyst supported on silica in the region 600 to 1100 wavenumbers. In rest the catalyst has a V=O stretch vibration at 1033 cm^{-1}. Exposure of the catalyst to a methanol/oxygen mixture leads to sharp bands appearing at 1067 and 1027 cm^{-1}. The same pattern holds for the data of a vanadium on alumina catalyst at low vanadium coverage and for vanadium on titania[23]. The peak at 1067 cm^{-1} can be assigned to a methoxy C-O stretch mode related to dissociative adsorption of methanol on silica and is thus irrelevant for the present discussion. The disappearance of the band at 1033 cm^{-1} indicates that the presence of unreacted -$VO(O_2)$ species on the support is reduced to an immeasurable concentration. A vibration at 1027 cm^{-1} appears in its place under reaction conditions, which is as predicted by the reaction mechanism presented here.

Thermodynamics

The energetics for the oxidative dehydrogenation of methanol, Figure 5.4, is just an energy diagram. The entropy as well as the enthalpy, effects are rather small, of the order of a few kT, which in atomic units is equal to 0.001 (2.6 kJ/mol) at 300K. Thus entropy or enthalpy effects are expected to be of minor importance.

5.4 Conclusions

The proposed mechanisms based on the umbrella model[7,8] for supported vanadium oxide catalyst in Figure 5.4 is a realistic route for the conversion of methanol in formaldehyde and water. In the first step a methanol molecule is converted into formaldehyde and water, with the removal of one oxygen atom from the -VO_3 species. In the second step this process is repeated, this leaves -VO. The catalyst is restored in step three to its original state by the addition of a gas phase oxygen molecule, -VO_3. This mechanism predicts a shift in the V=O vibrational frequency which is indeed seen both under catalytic reaction conditions.

References

(1) Amiridis, M. D.; Wachs, I. E.; Deo, G.; Jehng, J.-M.; Kim, D. S. *J. Catal.* **1996**, *161*, 247.

(2) Bosch, H.; Janssen, F. J. J. G.; Kerkhof, F. M. G. v. d.; Oldenzieli, J.; Ommeni, J. G. v.; Ross, J. R. N. *Appl. Catal.* **1986**, *25*, 239.

(3) Lopez Nieto, J. M.; Concepcion, P.; Dejoz, A.; Knözinger; Melo, F.; Vazquez, M. I. *J. Catal.* **2000**, *189*, 147.

(4) Wada, K.; Yamada, H.; Watanabe, Y.; Mitsudo, T.-A. *J. Chem. Soc., Faraday Trans.* **1998**, *94*, 1771.

(5) Zhu, Z.; Liu, Z.; Liu, S.; Niu, H. *Appl. Catal. B* **1999**, *23*, 299.

(6) Weckhuysen, B. M.; Keller, D. E. *Catal. Today* **2003**, *78*, 25.

(7) Gijzeman, O. L. J.; van Lingen, J. N. J.; van Lenthe, J. H.; Tinnemans, S. J.; Keller, D. E.; Weckhuysen, B. M. *Chem. Phys. Lett.* **2004**, *397*, 277.

(8) van Lingen, J. N. J.; Gijzeman, O. L. J.; van Lenthe, J. H.; Weckhuysen, B. M. *J. Catal.* **2006**, *239*, 34.

(9) Chen, K.; Iglesia, E.; Bell, A. T. *J. Catal.* **2000**, *192*, 197.

(10) Takahara, I.; Saito, M.; Inaba, M.; Murata, K. *Catal. Lett.* **2005**, *102*, 201.

(11) Deo, G.; Wachs, I. E. *J. Catal.* **1994**, *146*, 323.

(12) Hess, C.; Drakec, I. J.; Hoefelmeyera, J. D.; Tilleya, T. D.; Bell, A. T. *Catal. Lett.* **2005**, *105*, 1.

(13) Khaliullin, R. Z.; Bell, A. T. *J. Phys. Chem. B* **2002**, *106*, 7832.

(14) Döbler, J.; Pritzsche, M.; Sauer, J. *J. Am. Chem. Soc.* **2005**, *127*, 10861.

(15) Zhanpeisov, N. U. *Res. Chem. Intermed.* **2004**, *30*, 133.

(16) Guest, M. F.; Bush, I. J.; van Dam, H. J. J.; Sherwood, P.; Thomas, J. M. H.; van Lenthe, J. H.; Havenith, R. W. A.; Kendrick, J. *Mol. Phys.* **2005**, *103*, 719.

(17) Hertwig, R. H.; Koch, W. *Chem. Phys. Lett.* **1997**, *268*.

(18) Stephens, P. J.; Devlin, F. J.; Chabalowski, C. F.; Frisch, M. J. *J. Phys. Chem.* **1994**, *98*.

(19) Dmitrenko, O.; Huang, W.; Polonova, T. E.; Francesconi, L. C.; Wingrave, J. A.; Teplyakov, A. V. *J. Phys. Chem. B* **2003**, *107*, 7747.

(20) Scott, A. P.; Radom, L. *J. Phys. Chem.* **1996**, *100*, 16502.

(21) Wong, M. W. *Chem. Phys. Lett.* **1996**, *256*, 391.

(22) McQuarrie, D. A. *Statistical Mechanics*; Harper & Row: New York, Evanston, San Fransico, London, 1976.

(23) Burcham, L. J.; Deo, G.; Gao, X.; Wachs, I. E. *Top. Catal.* **2000**, *11/12*, 85.

(24) Gao, X.; Wachs, I. E. *J. Phys. Chem. B* **2000**, *104*, 1261.

(25) Stiegman, A. E.; Eckert, H.; Plett, G.; Kim, S. S.; Anderson, M.; Yavrouian, A. *Chem. Mater.* **1993**, *5*, 1591.

Chapter 6

A note on the calculation of analytical Hessians in the Zeroth Order Regular Approximation (ZORA)

Abstract

The previously proposed atomic ZORA approach, which was shown to eliminate the gauge dependent effect on gradients and to be remarkably accurate for geometry optimizations, is tested for the calculation of analytical second derivatives. It is shown that the resulting analytic second derivatives are indeed exact within this approximation. The method proves to yield frequencies that are remarkably close to the experimental frequency for uranium hexafluoride but less satisfactory for the gold dimer.

Published in: van Lenthe, J.H.; van Lingen, J. N. J. Int. J. Quantum Chem. 2006, 106, 2525.

6.1 Introduction

For highly accurate quantum chemical calculations the effects of relativity can hardly be ignored. Relativistic effects may be crucial to explain the reaction dynamics when heavy elements, of special interest in catalysis, are involved, even at Hartree-Fock or DFT level. The Zeroth Order Relativistic Approximation[1,2] was rediscovered in the nineties[3-5] and has recently again experienced a surge of interest[6,7]. This approach in its simplest scalar form reduces the Dirac equation[8] to a one component equation where the kinetic energy operator is replaced by a potential dependent operator.

$$\frac{p^2}{2m} \Rightarrow p \cdot \frac{1}{2c^2 - V} \cdot p \tag{6.1}$$

Matrix elements of the kinetic energy operator thus become[9]:

$$(T^{ZORA})_{\mu\nu} = \left\langle \phi_\mu \middle| p \cdot \frac{1}{2c^2 - V} \cdot p \middle| \phi_\nu \right\rangle \tag{6.2}$$

Where V is the Coulomb potential due to electrons and nuclei. In the context of DFT theory the inverse operator is generally determined using numerical integration. In our approach we have used a resolution of the identity operator employing a suitably chosen orthogonalised internal basis and a matrix inversion[10]. To recover the correct relativistic limit, the kinetic energy operator is split of.

$$\begin{aligned}(T^{ZORA})_{\mu\nu} = &-\frac{1}{2}\langle \phi_\mu | p^2 | \phi_\nu \rangle - \frac{1}{2}\sum_\lambda \left\langle \phi_\mu \middle| \vec{p} \middle| \phi_\lambda \right\rangle \left\langle \phi_\lambda \middle| \vec{p} \middle| \phi_\mu \right\rangle + \\ &+ \frac{1}{2}\sum_{\kappa\lambda} \left\langle \phi_\mu \middle| \vec{p} \middle| \phi_\lambda \right\rangle \left\langle \phi_\lambda \middle| \frac{2c^2 - V}{2c^2} \middle| \phi_\kappa \right\rangle^{-1} \left\langle \phi_\kappa \middle| \vec{p} \middle| \phi_\nu \right\rangle\end{aligned} \tag{6.3}$$

A major problem plaguing this operator is the fact that the presence of the potential in the inverse coulomb operator causes a lack of gauge invariance, i.e. if a constant is added to the potential this constant is not properly reproduced in the total energy. In our previous paper[11] we therefore proposed to calculate the ZORA corrections separately for the atoms. To eliminate all dependence on the atomic coordinates both the potential and all matrix elements are calculated just for the atoms. Thus we use

$$(T^{ZORA})_{\mu\nu} = -\frac{1}{2}\langle \phi_\mu | p^2 | \phi_\nu \rangle - \frac{1}{2}\left\{ \begin{array}{l} \sum_\lambda \left\langle \phi_\mu \middle| \vec{p} \middle| \phi_\lambda \right\rangle \left\langle \phi_\lambda \middle| \vec{p} \middle| \phi_\nu \right\rangle - \\ \sum_{\kappa\lambda} \left\langle \phi_\mu \middle| \vec{p} \middle| \phi_\lambda \right\rangle \left\langle \phi_\lambda \middle| \frac{2c^2 - V_{Atom}}{2c^2} \middle| \phi_\kappa \right\rangle^{-1} \left\langle \phi_\kappa \middle| \vec{p} \middle| \phi_\nu \right\rangle \end{array} \right\}_{Atom} \tag{6.4}$$

The relativistic corrections to the kinetic energy matrix elements may thus be calculated separately for each unique atom or even stored, requiring negligible computing time. Subse-

quently they are only added to the kinetic energy integrals for basis functions that are both centered on the atom concerned. This way the influence of the potential of other atoms is completely eliminated, curing the gauge problem resulting from this potential. Also as the ZORA corrections move with the atoms, they have no other effect on the gradients than the change in the wavefunction due to the different kinetic energy operator. Thus no special gradient related terms need to be programmed. The reasoning that no extra terms enter our gradient expressions can be applied to the second derivatives as well. As the ZORA corrections move with the atoms no second derivatives of these corrections are required. The approach proved to be very accurate[11], as the elimination of the Gauge dependence well outweighs the minor effect of the other atoms on the atomic potential.

Other methods have been proposed to facilitate the calculation of gradients within the ZORA formalism. They include using a model potential[5], to allow analytic expressions for the gradients and applying corrections to the potentials to approximately eliminate the influence of the other atoms[6,12]. None of these methods, including our atomic ZORA is Gauge independent in a general sense. An extension of our atomic idea to the case of e.g. polarisabilities would entail just ignoring the electric field in the evaluation of the ZORA correction.

6.2 Calculations

To illustrate the effectiveness of the method we performed calculations on the vibrational states of Au_2, CsI and UF_6. We present both Hartree-Fock and DFT (B3LYP[13,14]) results. For UF_6 we also calculated vibrational modes using a pseudo-potential employing LanL2DZ, expecting little effect of the ZORA corrections. For a real life application we estimate the relevance of relativity for the vibrational spectrum of a V-O catalyst on a silica surface.

For Au and CsI we use a basis employed previously[11]. For Uranium we employed an even tempered basis set akin to a relativistic basis set of Koga et al[15], whereas a DZVP basis was employed for fluorine. For the vanadium oxide umbrella structure[16] two basis sets (LanL2DZ and TZVP) were used.

The calculations were performed with the GAMESS-UK program[17]. In all cases the ZORA corrections were calculated for Hartree-Fock atoms.

6.3 Results and discussion

In Table 6.1 we give a comparison of analytical and finite-difference Hessians, calculated with a 2-point approach (FORCE), for Au_2 and CsI. The errors were similar to those in non-relativistic calculations and must be due to the limited accuracy of the FORCE calculation. The atomic ZORA corrections depend on the atomic density, since the electron repulsion is contained in the atomic potential V. For gold the resulting iteration process took up to

Table 6.1 Comparison of frequencies from analytical Hessians and 2-point force calculations for CsI and Au_2. Experimental data for CsI[21] and Au_2[22,23]. Vibrations in cm^{-1} and distances in Å.

	Au_2			CsI		
	R	Hessian	FORCE	R	Hessian	FORCE
HF	2.879	104.63	104.67	3.563	104.44	105.68
HF-ZORA	2.676	141.53	141.45	3.520	105.94	106.74
B3LYP	2.779	124.33	124.43	3.469	107.06	106.92
B3LYP-ZORA	2.621	154.92	154.78	3.435	108.09	108.18
Exp	2.472	190.9			113.9	

7 iterations to converge to 10^{-6}, while the total energy reduced from -39720.120329 to -39277.970266 Hartree, compared to a non-relativistic value of -35696.119946. This suggests a considerable effect of the electron-electron repulsion on the final ZORA corrections. Though ZORA does show an improvement compared to experiment, the calculated frequencies are still significantly off. Comparison with more extended calculations[18] suggests, that higher order relativistic corrections and more extended correlation treatment is required for this weakly bonded system. The DK3 treatment in ref.[18] raises the frequency by some 60 cm^{-1}, compared to 40 cm^{-1} for ZORA, whereas CCSD(T) adds another 30 cm^{-1}, compared to 20 cm^{-1} for DFT.

Table 6.2 Calculated equilibrium distance and vibrational modes for UF_6 with experimental data[19,20]. Vibrations in cm^{-1} and distance in Å.

UF_6	R	a_{1g}	e_g	t_{1u}	t_{1u}	t_{2g}	t_{2u}
HF	1.982	665	300	593	164	235	122
HF-ZORA	1.988	740	551	665	198	220	145
B3LYP	2.038	563	430	553	127	192	125
B3LYP-ZORA	2.012	664	546	628	181	194	138
B3LYP-LanL2DZ	2.019	632	527	620	171	188	146
B3LYP-LanL2DZ-ZORA	2.019	627	523	618	168	188	146
Exp.	1.999	676	534	626	186	200	143

For the most relativistic molecule UF_6 (Table 6.2), depending on the vibrational mode, the effects of adding DFT and adding relativity sometimes go in the same direction and sometimes cancel. The net effect is that each one on its own performs rather poorly, showing deviations from experiment[19,20] ranging from 234 cm^{-1} (HF) and 113 cm^{-1} (B3LYP). Combining the DFT with the atomic ZORA gives a remarkable agreement with experiment, a deviation of only 12 cm^{-1}. The pseudo-potential calculations, named LanL2DZ, show quite acceptable frequencies in comparison with experiment; The ZORA corrections do not show improvement.

Calculations on the umbrella model[16] gave the results shown in Table 6.3. From this table it is quite clear that the ZORA corrections have a small influence on the frequencies of the V=O stretch and O-O stretch in the peroxo group, depending of the basis set. As is to be expected, the LanL2DZ ecp basis set shows the smallest differences since its core is already fitted to a relativistic one and cannot be changed by ZORA. The TZVP lower the O-O vibration by 2 cm^{-1} and increases the V=O frequency by 4 cm^{-1}. This basis places the O-O stretch at approximately 940 cm^{-1} which compares well with the experimental value[16]. The difference between the LanL2DZ result and that produced with the TZVP basis indicates, that the lack of polarization functions is far more serious then any effect of relativity on the vibrations.

Table 6.3 Calculations on the vanadium oxide cluster. Energy in a.u, vibrations in cm^{-1}.

	LanL2DZ		TZVP	
Energy	non-relativistic	ZORA	non-relativistic	ZORA
atomic	-1286.1740379	-1287.4018909	-3299.1601219	-3311.4407690
total	-1296.4430835	-1297.6638687	-3312.2795414	-3324.5615891
vibrations				
O-O	912.37	913.05	944.56	941.63
V=O	1103.87	1103.95	1086.11	1089.98

6.4 Conclusion

We have shown that the Atomic ZORA approach is able to generate exact analytical HESSIANS. As the approach completely avoids the gauge problems associated with molecular ZORA calculations, the results are significantly more accurate than a molecular ZORA could be. Test calculations on UF_6 show remarkable agreement with experiment if both DFT and ZORA are enabled. The lack of relativistic effects in the standard calculations on supported vanadium oxides seems a justified approximation.

References

(1) Chang, C.; Pelissier, M.; Durand, P. *Phys. Scr.* **1986**, *34*, 394.
(2) Heully, J. L.; Lindgren, I.; Lindroth, E.; Lundqvist, S.; Maartensson-Pendrill, A. M. *J. Phys. B: At., Mol. Opt. Phys.* **1986**, *19*, 2799.
(3) Faas, S.; Snijders, J. G.; van Lenthe, J. H.; van Lenthe, E.; Baerends, E. J. *Chem. Phys. Lett.* **1995**, *246*, 632.
(4) van Lenthe, E.; Baerends, E. J.; Snijders, J. G. *J. Chem. Phys.* **1994**, *101*, 9783.
(5) van Wüllen, C. *J. Chem. Phys.* **1998**, *109*, 392.
(6) Filatov, M.; Cremer, D. *J. Chem. Phys.* **2005**, *122*, 44104.
(7) Sadlej, A. J. *Collect. Czech. Chem. Commun.* **2005**, *70*, 677.
(8) Dirac, P. A. M. *Proc. Roy. Soc. (London)* **1928**, *A118*, 351.
(9) van Lenthe, E.; Van Leeuwen, R.; Baerends, E. J.; Snijders, J. G. *Int. J. Quantum Chem.* **1996**, *57*, 281.
(10) Faas, S.; Snijders, J. G.; Van Lenthe, J. H. *Prog. Theor. Chem. Phys.* **2000**, *2*, 251.
(11) van Lenthe, J. H.; Faas, S.; Snijders, J. G. *Chem. Phys. Lett.* **2000**, *328*, 107.
(12) van Lenthe, E.; Ehlers, A.; Baerends, E.-J. *J. Chem. Phys.* **1999**, *110*, 8943.
(13) Hertwig, R. H.; Koch, W. *Chem. Phys. Lett.* **1997**, *268*, 345.
(14) Stephens, P. J.; Devlin, F. J.; Chabalowski, C. F.; Frisch, M. J. *J. Phys. Chem.* **1994**, *98*, 11623.
(15) Koga, T.; Tatewaki, H.; Matsuoka, O. *J. Chem. Phys.* **2003**, *119*, 1279.
(16) Gijzeman, O. L. J.; van Lingen, J. N. J.; van Lenthe, J. H.; Tinnemans, S. J.; Keller, D. E.; Weckhuysen, B. M. *Chem. Phys. Lett.* **2004**, *397*, 277.
(17) Guest, M. F.; Bush, I. J.; Van Dam, H. J. J.; Sherwood, P.; Thomas, J. M. H.; Van Lenthe, J. H.; Havenith, R. W. A.; Kendrick, J. *Mol. Phys.* **2005**, *103*, 719.
(18) Tsuchiya, T.; Abe, M.; Nakajima, T.; Hirao, K. *J. Chem. Phys.* **2001**, *115*, 4463.
(19) Hay, P. J.; Martin, R. L. *J. Chem. Phys.* **1998**, *109*, 3875.
(20) Schreckenbach, G.; Hay, P. J.; Martin, R. L. *J. Comput. Chem.* **1999**, *20*, 70.
(21) Konings, R. J. M.; Booij, A. S.; Cordfunke, E. H. P. *Vib. Spectrosc.* **1991**, *2*, 251.
(22) Wang, F.; Liu, W. *Chem. Phys.* **2005**, *311*, 63.
(23) Wang, X.; Wan, X.; Zhou, H.; Takami, S.; Kubo, M.; Miyamoto, A. *J. Mol. Struc. (Theochem)* **2002**, *579*, 221.

Chapter 7

Future prospects

In the previous Chapters the umbrella model for the supported vanadium oxide catalyst, has been discussed and compared with other models for supported vanadium oxide catalyst. Although the umbrella model has experimental support, there is no clear evidence that this is the only molecular structure present on the surface of the support. More research is thus required. With respect to a further elucidation of the molecular structure the following experiments and calculations could be performed:

In Chapter 3 we calculated that the perturbed oxygen molecule is attached to the vanadium with a bond energy of -352.3 kJ/mol. This means that in vacuum environment it will detach when the catalyst is heated to around 800 or 900 °C. When the oxygen has departed, the active species only consist of a -O-V=O, which should not have the O-O stretch normal mode at 920 cm^{-1}. So the heated catalyst in vacuum does not shows a 920 cm^{-1} band. Of course we may have overestimated the bond strength and the oxygen molecule desorbs at a lower temperature or even at reaction temperatures of 200 - 500 °C. As catalysis takes place under flowing oxygen, there will always be an oxygen molecule around that will stick to the active -V=O species on the support surface and this will be seen in the spectra. Thus, if the 920 cm^{-1} band disappears at 200-500 °C under vacuum, it should be reappear under the flowing oxygen.

Chapter 4 has shown that the synthesis method is very important for the final molecular structure of the species. It will therefore be very interesting to investigate the synthesis process with Raman and IR to see what kind of processes are taking place. For example what is the structure of the vanadium oxide species in the solvent before and during the incipient wetness impregnation. Is this species in solution attached to the surface of the support when the solution is in contact with the support or does the adsorption take place when the solvent is almost evaporated. Good tools for this study would be Raman and IR. Models structure for the species in the solution have already be calculated and can be easily compared with experimental spectra.

In this thesis the main focus point has been on Raman and IR. At low loadings the spectrum of the silica support is very dominant in the regions of interest, which makes it difficult to assign peaks. Other spectroscopic techniques might help. As shown in the general introduction NMR and UV-VIS characteristics may be calculated. A preliminary theoretical study into these techniques has shown that there are some interesting characteristics for the models described. In case of the ^{51}V NMR the shift of the dehydrated umbrella model is quite different from the other models presented.

Regarding UV-VIS it has already been shown that the vanadium oxide catalyst is white in dehydrated state. This means that the catalyst absorbs in the UV range. When the catalyst is hydrated the original white color is replaced by orange and ultimately dark red. So there is quite a large shift in absorption wavelength. As this process is reversible, this means that the

water molecule is only adsorbed to the active species probably via some dipole interaction. The UV-VIS spectra of the species can be calculated by RPA calculations on the models with or without water, which will give the electronic transitions for the models simulated.

The effect of the support clusters seems to be of minor importance for the structure of the umbrella model. For kinetics this may not be true as binding energies may change slightly. It would therefore be interesting to set up a QM/MM model with ChemShell or any other program that is able to combine the Quantum Mechanics part with the Molecular Mechanics part.

Although the structure is still under debate, it is interesting to look at possible reaction mechanisms. In Chapter 5 a reaction mechanism is presented for the conversion of methanol to formaldehyde based on the umbrella model. From this reaction mechanism experiments can be deduced to learn more about the reaction mechanism:

As simple experiment would be to let the catalyst work without the oxygen environment. This will stop the reaction at some stage. In the case of the umbrella model the reaction can go on for two cycles producing two formaldehyde molecules per active site. With the traditional reaction mechanism, which involves a surface oxygen, this is only one formaldehyde molecule per active site before the reaction stops.

It could also be interesting to replace the oxygen in the silica support with ^{18}O. In our reaction mechanism only oxygen of the active species are used which means that in the products only ^{16}O should be present. In the other reaction mechanisms a support oxygen is used so ^{18}O would be present in the products.

In Chapter 5, only minima are presented in the reaction mechanism. This is because we have not found the most essential transition states yet. These are needed to allow conclusions regarding the activation energy and the kinetics of the reaction. Extra work on finding the transition states between the minima is essential for a good understanding of the mechanism.

From a more theoretical view the last step in the reaction mechanism proposed in Chapter 5 is very interesting. In this step the spin changes from a triplet state to a singlet state. This probably will happen when the oxygen molecule approaches the vanadium oxide species. So along this reaction coordinate there should be an avoided crossing. To study this together with the relativistic character the vanadium oxide species will help us to get more insight in the reaction mechanism and more specific this transfer from triplet to singlet. A first study into that in Chapter 6 only considers the scalar relativistic operator. This study has to be extended with spin orbit coupling since that is the part involved with the relaxing of the selection rules which makes this spin flip possible.

Chapter 8

Summary en Samenvatting

Summary

Supported vanadium oxide catalysts are widely used in industry. However, the molecular structure of the active species, responsible for the actual catalysis, is for a large part still unknown. This thesis describes four years study on the elucidation of this molecular structure. It mainly focuses on the umbrella model (Figure 8.1). This model was introduced by Dr. Gijzeman as an alternative to models already present in the literature. In this model the vanadium atom is linked to the surface via only one Si-O_s-V bond and further consists of a V=O and a perturbed O_2 molecule linked to the central vanadium atom. Spectroscopic characteristics (Raman, IR) for the umbrella model have been calculated for two types of support, alumina and silica, and compare very well with experimental data found in the literature. From this comparison it could be concluded that the umbrella model is able to assign vibrations to the observed peaks at 900, 980 and 1040 cm^{-1} and can also explain the width of the peaks (Chapters 2 and 3).

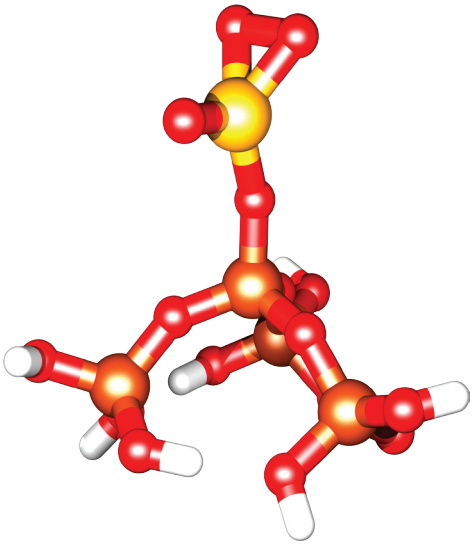

Figure 8.1 The umbrella model.

A comparison between several model structures, the umbrella models and three alternative models from literature, has been made against experimental Raman and IR spectra (Chapter 4). It could be concluded that the method of synthesis has an influence on the type of active species on the support.

Regarding the conversion of methanol to formaldehyde, one of the processes for which this catalyst is used, a plausible reaction mechanism has been presented based on the umbrella model (Chapter 5). Basically it involves three steps. In the first step a methanol molecule is converted into formaldehyde and water, with the removal of one oxygen atom from the -VO_3 species. In the second step this process is repeated, which leaves a -VO species that can readily reactivated by the attachment of a whole oxygen molecule. For this last step to be possible spin orbit coupling, a relativistic property, is needed. A first study into the relativistic properties of the vibrations of molecules has been done (Chapter 6).

Samenvatting

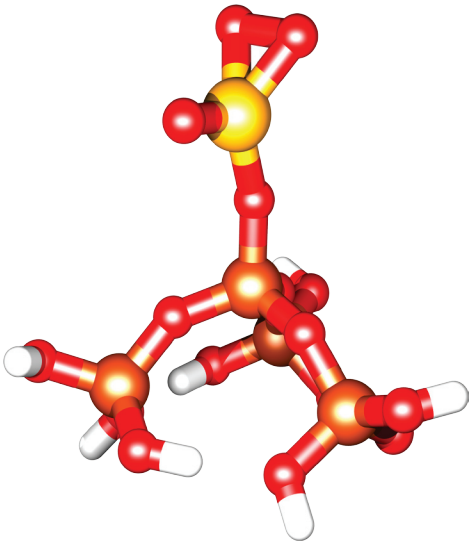

Figurur 8.2 Het paraplu model.

Gedragen vanadium oxide katalysatoren worden veel gebruikt in de industrie. Echter, de moleculaire structuur van het actieve gedeelte, verantwoordelijk voor de feitelijke katalyse, is grotendeels nog steeds onbekend. Dit proefschrift beschrijft vier jaren van studie tot verheldering van deze moleculaire structuur. Het richt zich hoofdzakelijk op het paraplu model (Figuur 8.2). Dit model is geïntroduceerd door Dr. Gijzeman als een alternatief voor de modellen, die al in de literatuur aanwezig waren. In dit model is het vanadium atoom verbonden met het oppervlak via een enkele Si-O_s-V binding en verder bestaat het uit een V=O en een verzwakt O_2 molecuul verbonden met het centrale vanadium atoom. Spectroscopische karakteristieken (Raman, IR) zijn uitgerekend voor het umbrella model gedragen op twee type dragermateriaal, alumina en silica. De resultaten komen goed overeen met experimentele gegevens gevonden in de literatuur. Uit deze vergelijking kon worden geconcludeerd dat het umbrella model in staat is om vibraties toe te wijzen aan waargenomen pieken op 900, 980 en 1040 cm^{-1} en ook de breedte van deze pieken kan verklaren (Hoofdstukken 2 en 3).

Er is een vergelijking gemaakt tussen verschillende model structuren, het umbrella model en drie alternatieve modellen uit de literatuur, en experimentele Raman en IR spectra (Hoofdstuk 4). Geconcludeerd kon worden dat de methode van synthese een invloed heeft op het type van de actieve structuur op de drager.

Voor de omzetting van methanol in formaldehyde, één van de processen waarvoor de katalysator wordt gebruikt, wordt een plausibel reactiemechanisme gepresenteerd op basis van het umbrella model (Hoofdstuk 5). Het omvat drie fundamentele stappen. In de eerste stap wordt een methanol molecuul omgezet in formaldehyde en water, met de verwijdering van een zuurstof atoom van de -VO_3 structuur. In de tweede stap wordt dit proces herhaald zodat er een -VO structuur overblijft, die makkelijk gereactiveerd kan worden door een nieuwe binding met een zuurstof molecuul aan te gaan. Spin-baan koppeling, een relativistische eigenschap, is nodig om deze laatste stap te laten verlopen. Een eerste studie naar de relativistische eigenschappen van vibraties van moleculen is uitgevoerd (Hoofdstuk 6).

List of publications

- van Oijen, A. M.; Verberk, R.; Durand, Y.; Schmidt, J.; van Lingen, J. N. J.; Bol, A. A.; Meijerink, A., *Continuous-wave two-photon excitation of individual CdS nanocrystallites*, Appl. Phys. Lett. **2001**, 79, 830.
- van Sark, W. G. J. H. M.; Frederix, P. L. T. M.; van den Heuvel, D. J.; Gerritsen, H. C.; Bol, A. A.; van Lingen, J. N. J.; de Mello Donega, C.; Meijerink, A., *Photooxidation and Photobleaching of Single CdSe/ZnS Quantum Dots Probed by Room-Temperature Time-Resolved Spectroscopy,* J. Phys. Chem. B **2001**, 105, 8281.
- van Sark, W. G. J. H. M.; Frederix, P. L. T. M.; van den Heuvel, D. J.; Bol, A. A.; van Lingen, J. N. J.; de Mello Donega, C.; Gerritsen, H. C.; Meijerink, A., *Time-Resolved Fluorescence Spectroscopy Study on the Photophysical Behavior of Quantum Dots*, J. Fluoresc. **2002**, 12, 69
- Gijzeman, O. L. J.; van Lingen, J. N. J.; van Lenthe, J. H.; Tinnemans, S. J.; Keller, D. E.; Weckhuysen, B. M., *A new model for the molecular structure of supported vanadium oxide catalysts,* Chem. Phys. Lett. **2004**, 397, 277.
- Nenu, C. N.; van Lingen, J. N. J.; Groot, F. M. F. d.; Koningsberger, D. C.; Weckhuysen, B. M., *Controlled Assembly of a Heterogeneous Single-Site Ethylene Trimerization Catalyst as Probed by X-ray Absorption Spectroscopy,* Chem. Eur. J. **2006**, 12, 4756.
- van Lenthe, J. H.; van Lingen, J. N. J., *Note on the Calculation of Analytical Hessians in the Zeroth-Order Regular Approximation (ZORA), I*nt. J. Quantum Chem. **2006**, 106, 2525.
- van Lingen, J. N. J.; Gijzeman, O. L. J.; van Lenthe, J. H.; Weckhuysen, B. M., *On the Umbrella Model for Supported Vanadium Oxide Catalysts,* J. Cat. **2006**, 239, 34.
- van Dam, H. J. J.; Guest, M. F.; Sherwood, P.; Thomas, J. M. H.; van Lenthe, J. H.; van Lingen, J. N. J.; Bailey, C. L.; Bush, I. J., *Large scale electronic structure calculations in the study of the condensed phase,* J. Mol. Struc: THEOCHEM, **2006**, 771, 33.

Dankwoord

Het probleem met dankwoorden is altijd dat er mensen vergeten worden en dat je die dan onbedoeld beledigd. Ik heb daarom lang getwijfeld of ik wel een dankwoord zou schrijven. ik heb daarom de volgende clausule bedacht:

Ter voorkoming van mogelijke aanslagen op mijn persoon, bedankt iedereen, maar dan ook echt iedereen, die mij op welke manier dan ook heeft geholpen bij de totstandkoming van dit proefschrift. Thanks to everyone that helped me in any way with completing my thesis.

Zo nu ik hopelijk niet meer hoofdelijk aansprakelijk kan worden gesteld voor het ontbreken van personen wil toch overgaan om mensen wat specifieker te bedanken. Om te beginnen mijn promotor Prof Weckhuysen en ook eigenlijk Wim Klopper. Zij hebben mij de mogelijkheid gegeven om aan deze promotie bij twee vakgroepen te beginnen. Bert bedankt voor alle vrijheid die je mij hebt gegeven. De bedoeling was dat ik zowel theoretisch als experimenteel werk zou doen. Dit is een klein beetje anders gelopen. Tevens vind ik het nog steeds jammer dat we niet meer aan de Cr_xO_y-katalysator hebben kunnen doen. Deze structuur is nog steeds een raadsel voor mij. Gelukkig zijn we veel verder gekomen met de VO_4-katalysator.

Dat brengt mij bij het dagelijkse management team. Joop, of moet ik manager in opleiding zeggen, bedankt dat je mijn promotie zo fantastisch hebt opgepakt nadat Wim was vertrokken. Op dat moment was er nog niet veel nuttigs gebeurd, maar ik denk dat we veel van die verloren tijd goed hebben gemaakt. Jij hebt structuur weten aan te brengen in mijn onderzoek. Alleen doe mij en de promovendi na mij een plezier en **koop nooit meer een HP.** Onno, 3 jaar geleden besloot jij eens de boel op zijn kop te zetten, iets wat jou niet vreemd is. Dit leidde tot het paraplu model en de rest is te vinden in dit boekje. Gaande weg ben jij steeds meer betrokken geraakt met mijn werk en hebben wij samen heel wat uurtjes door gebracht met het bestuderen van de resultaten van onze berekeningen. Blijkbaar was dit zo gezellig dat je besloot na je vroegtijdig pensioen, een klein jaar geleden, bij mij op de kamer bij theoretische chemie te komen zitten. Joop, Onno super bedankt voor alle hulp en ondersteuning bij mijn promotie en de soms religieuze discussies met de beoordelaars van onze artikelen.

Henk, je was mijn enige hoofdvakstudent, we zijn helaas niet ver genoeg gekomen met de overgang van triplet naar singlet om het op te nemen in dit proefschrift. Ik stond verbaasd over de enorme stappen die je hebt genomen in je leven dat jaar. Veel succes met je promotie in Engeland en bedankt voor de vele “misschien iets te diepe” discussies.

Remco, Paul bedankt voor jullie interesse in mijn werk, de prettige samenwerking en jullie deskundige oordeel. Jeroen, Petar en Henri zonder jullie was het lang niet zo gezellig geweest in de groep en onze wintertrips naar Han. Huub, Paul, Jens, thanks for the great

time and all the help I had in Daresbury.

In de anorganische groep wil ik voornamelijk Ingmar, Rudy en Vincent bedanken voor hun discussies over berekeningen en computers. Ingmar ik geef aan jou het stokje door om de anorganische gemeenschap wat bij te brengen over de mogelijkheden van de quantum chemie.

Cristina, we shared some crazy last months before our thesises were send to the reading committee. Working with you on two chapters/articles was very interesting and challenging to me. Thanks for this!

Tot slot wil ik mijn ouders en mijn zusje bedanken voor de mentale ondersteuning, jullie wisten mij altijd weer op te beuren als ik humeurig thuis kwam. Zonder jullie was dit proefschrift er niet geweest.

Joost

Over de auteur

Joost Nelis Johannes van Lingen werd geboren op 29 oktober 1977 te Zeist. In 1996 behaalde hij het eindexamen VWO aan het Christelijk Gymnasium te Utrecht. In datzelfde jaar is hij een studie Scheikunde begonnen aan de Universiteit Utrecht. Na het doen van een bijvak bij de sectie Fysische en Colloid Chemie en een hoofdvak bij de sectie Gecondenseerde Materie studeerde hij met genoegen af. Tijdens zijn studie liep hij stage op het Natuurkundige Laboratorium van Philips Research in Eindhoven.

Vanaf 2002 was hij werkzaam als assistent in opleiding bij de Faculteit Scheikunde van de Universiteit Utrecht in de secties Anorganische Chemie en Katalyse o.l.v. Prof. Dr. Ir. B.M. Weckhuysen en de sectie Theoretische Chemie o.l.v. Dr. J.H. van Lenthe en Dr. O.L.J. Gijzeman. Het onderzoek dat sinds die tijd is uitgevoerd heeft geleid tot dit proefschrift.